Hong, Gonghua; Cheng, Haitao; Zhang, Shuangbao; Rojas, Orlando J.

Polydopamine-treated hierarchical cellulosic fibers as versatile reinforcement of polybutylene succinate biocomposites for electromagnetic shielding

Published in:
Carbohydrate Polymers

DOI:
10.1016/j.carbpol.2021.118818

Published: 01/02/2022

Document Version
Peer-reviewed accepted author manuscript, also known as Final accepted manuscript or Post-print

Polydopamine-treated hierarchical cellulosic fibers as versatile reinforcement of polybutylene succinate biocomposites for electromagnetic shielding

Gonghua Hong [a,b,c], Haitao Cheng [e], Shuangbao Zhang [a,b,*], and Orlando J. Rojas [c,d,*]

[a] Beijing Key Laboratory of Wood Science and Engineering, Beijing Forestry University, Beijing 100083, China
[b] MOE Key Laboratory of Wooden Material Science and Application, Beijing Forestry University, Beijing 100083, China
[c] Department of Bioproducts and Biosystems, Aalto University, Vuorimiehentie 1, Espoo, P.O. Box 16300, FI-00076 Aalto, Finland
[d] Bioproducts Institute, Department of Chemical & Biological Engineering, Department of Chemistry, and Department of Wood Science, The University of British Columbia, 2360 East Mall, Vancouver, BC V6T, 1Z3, Canada
[e] Bamboo and Rattan Science and Technology Key Laboratory of the State Forestry Administration, International Centre for Bamboo and Rattan, Beijing 100102, PR China

[*] Corresponding author:
Shuangbao Zhang: shuangbaozhang@163.com
Orlando J. Rojas: orlando.rojas@ubc.ca

ABSTRACT

There is a need for scalable technologies to reduce electromagnetic pollution with materials of low density and low carbon footprint. Unfortunately, environmental adaptability, economic feasibility and lightweight are factors that are still far from optimal in most electromagnetic shielding materials. Herein, we address these challenges with polybutylene succinate (PBS) reinforced with bamboo fibers functionalized with Fe_3O_4 nanoparticles (Fe_3O_4-NPs) and polypyrrole (PPy). Such hybrid system was compatibilized *via* polydopamine (PDA) coupling, demonstrating magnetic, dielectric and interfacial polarization losses as well as distributed reflection, yielding a shielding effectiveness of ~36.9 dB. Simultaneously, the composite displayed gains in tensile strength and modulus (by 18 and 38%, respectively) combined with improved flexural strength and modulus (by 33% and 15%, respectively). Overall, this work demonstrates a new pathway toward low cost and lightweight bio-based materials for high-performance electromagnetic shielding.

Keywords: cellulosic fibers, biocomposites, absorption-type electromagnetic shielding, surface functionalization, polydopamine coupling

1. Introduction

The rapid growth of intelligent technologies and the widespread use of electronic devices have improved communication and quality of life. However, this is at the expense of pollution emissions that are inadvertently generated as electromagnetic

63 waves (EMW) (Markham, 1999; Wanasinghe, Aslani, Ma, & Habibi, 2020). Moreover,
64 the interactions between electronic devices and natural sources (lighting and solar flares)
65 typically produce electromagnetic interference (EMI), which not only cause
66 disturbances in the function of the electronic devices and electrical circuits, but result
67 in health hazards (Jiang et al., 2019; Kraz & Wallash, 2000; Singh, Shishkin, Koppel,
68 & Gupta, 2018). Associated risks include negative impacts in electrical transmission
69 lines, electric motors, radars, microwaves, household electric appliances and
70 telecommunication networks (Karteri, Altun, & Gunes, 2017; Madhu, Gurusiddesh,
71 Kiran, Shruthi, & Jayanna, 2016; Shen, Zhai, & Zheng, 2014; Wen et al., 2014). Overall,
72 there is an increased demand for materials that offer protection against EMI.

73 Metallic materials have gained popularity to shield EMI (Menon, Madras, & Bose,
74 2017; Zhang et al., 2019). However, apart from their poor environmental adaptability,
75 high density and costly processing, they generally cause secondary electromagnetic-
76 radiation (ER) pollution, *via* reflection, which undermines their adoption. Hence,
77 several efforts have been devoted to developing environmental protection and
78 lightweight absorption-type EMI shielding materials. For instance, low-density and
79 eco-friendly biopolymer composites based on carbon materials (including carbon black,
80 carbon fibers/nanofibers/nanotubes and graphene) or, alternatively, metallic
81 nanowires/nanoparticles (Ag, Cu, Ni and Fe) have received great attention in next-
82 generation EMI absorbing materials given that they can potentially meet the stringent
83 requirements of protection against secondary reflected ER pollution (Chauhan,
84 Abraham, & Choudhary, 2016; Ji et al., 2018; Ju et al., 2020; Khodiri, Al-Ashry, & El-

Shamy, 2020; Lecocq et al., 2020; Li et al., 2017; Liang, Ruan, Zhang, & Gu, 2020; Lin et al., 2016; Rengaswamy et al., 2018; Wang et al., 2018; Wu, Chen, Zhao, Liu, & Zhang, 2016; Yu, Dai, Yuan, Zou, & Liu, 2020; Zeng et al., 2017; Zhao, Fu, Chen, Zhong, & Wang, 2016).

To produce biopolymer-based composites with high EMI shielding effectiveness (SE), one of the most dependable solutions involve the addition of conductive and/or absorbing fillers. Unfortunately, fillers with poor dispersibility aggregate at high loadings, causing deterioration in mechanical performance. Hence, there is a need to address the trade-off between mechanical strength and EMI SE in polymer-based composites.

Cellulosic fiber-reinforced composites are desirable for their eco-friendliness, low density, lightweight and easy processing; thus, they have emerged as preferred choices in structural materials (Claramunt, Fernández-Carrasco, Ventura, & Ardanuy, 2016; Dahy, 2019; Gopinath, Poopathi, & Saravanakumar, 2019; Nurul Fazita et al., 2016). For EMI shielding, natural cellulosic fiber-reinforced polymer composites include coatings with well dispersed conductive and/or absorbing fillers; meanwhile, the desired mechanical and EMI shielding properties can be realized by proper reinforcement (Patterson & Sodano, 2016). Fibers randomly oriented in polymer matrices can form an interconnected network to generate distributed reflecting surfaces and restrain penetration of EMW into the substrate. Among the natural cellulosic fibers available, those from fast growing bamboo stand out for their low-cost, recyclability, mechanical strength and availability (Liu, Song, Anderson, Chang, & Hua, 2012; Tang,

Tian, & Hsu, 2015; Xu, Shamey, & Hinks, 2010). The -OH groups in the main constituents of the fibers, cellulose and hemicelluloses, orient along the direction the EMW oscillation, resulting in dipole relaxation and energy sinking. Furthermore, adsorption and multireflection generated from the fiber-based network synergistically act *via* dipole relaxation, further enhancing the EMI SE of the composite. To develop high-performance absorption-type shielding materials, suitable impedance matching and attenuation with appropriate permittivity and permeability are of essence. Considering that most electromagnetic materials display a dielectric constant that is much larger than the permeability, increasing the latter property and/or decreasing the dielectric constant are deemed as useful routes to achieve suitable impedance matching (*e.g.*, for satisfactory EMW absorption). For surface functionalization of bamboo fibers, *in-situ* deposition of Fe_3O_4 nanoparticles (Fe_3O_4-NPs) have gained recognition, given that it enhances EMI SE by virtue of valuable magnetic-loss-activated performance (Wang et al., 2011). Moreover, the excellent dielectric loss-activated capacity of polypyrrole (PPy) adds to EMI shielding (Geetha, Satheesh Kumar, Rao, Vijayan, & Trivedi, 2009; Zhan et al., 2018). Unfortunately, the anchoring strength between functional coatings and fibers remains challenging, causing losses during processing (for instance, during washing and manufacturing).

Recently, composites with good interfacial adhesion have been achieved by following the example of wet addition of mussel byssus. For instance, 3,4-dihydroxy-phenylalanine and lysine amino acids secreted by related organisms have shown high chemical reactivity, contributing to a superior adhesion (and cross-linking) ability (Lee,

Scherer, & Messersmith, 2006; Ye, Zhou, & Liu, 2011). Moreover, dopamine, a small catecholamine, can oxidatively self-polymerize in mild alkaline conditions into polydopamine (PDA). Hence, PDA coatings have been shown for interfacial modification of various materials (nanoparticles, nanowires, nanotubes, microbeads, and organisms, for instance) (He et al., 2017; He et al., 2019; Mumtaz et al., 2017; Sadjadi, Lazzara, Malmir, & Heravi, 2018; Yan et al., 2020; Zeng et al., 2017). Moreover, the catechol moiety in PDA coatings can directly immobilize metal ions on a variety of substrates*, e.g.,* for secondary reactions *via* chelation (Huang et al., 2016; Yan et al., 2013; Ye et al., 2011). Thus, mussel-inspired adhesion further our efforts for interfacial modification and represents a simple and feasible route to achieve natural fiber-reinforced polymer composites (Cheng, Chen, Wang, & Shie, 2016; Kalinke et al., 2020; Liu et al., 2020; Wang, Zhang, Chen, Zhang, & Fang, 2017; Zhang et al., 2017).

In EMI shielding applications, Liu and Liao (2020) designed an absorbing shielding nanocomposite by introducing Fe_3O_4-NPs and PPy coatings onto collagen fibers. Furthermore, Li *et al.* (2020) proposed a 3D graphene aerogel synthesized with Fe_3O_4-NPs and PPy that was effective against electromagnetic pollution. Despite the recent progress, there is still a need for simple, bionic strategy to achieve absorption-type natural cellulosic fiber-reinforced composites, for instance, functionalized with Fe_3O_4-NPs and PPy. In this study, we introduce a green and lightweight EMW shielding biocomposite using bio-based polybutylene succinate (PBS) and bamboo fibers functionalized by PDA-based surface coatings, forming an interconnected network within the matrix. In the process of fiber functionalization, magnetic-loss-activated

151 Fe_3O_4-NPs and dielectric loss-activated PPy were successively deposited on the
152 surfaces of the bamboo fibers. The complex coatings were investigated by SEM, FT-
153 IR, XPS and XRD. The performance of the functionalized fibers was assessed in terms
154 of the magnetic and dielectric losses, interfacial polarization loss and distributed
155 reflection, all of which were related to the fiber-based network and its ability to
156 dissipate EMW energy. The absorption-type shielding biocomposites were fabricated
157 through a simple hot-pressing procedure. The magnetic behavior, electrical and EMI
158 shielding performance, mechanical strength and interfacial interactions were examined.
159 The results confirmed that the obtained PBS-based biocomposites possess an excellent
160 irradiation absorption. Such performance is explained to be the result of dielectric and
161 magnetic losses, impedance matching, interface polarization as well as electron
162 migration produced by the interconnected conductive network. The results, coupled
163 with the lightweight, low-cost and green processing, indicate the promise of the
164 introduced material for large-scale applications in EMI shielding.
165
166 **2. Materials and methods**
167 *2.1 Materials*
168 PBS with a flow index, density and crystallinity of 2.0 g/10 min, 1.24 g/cm^3 and 32%,
169 respectively, was purchased from Showa Highpolymer Co. Ltd. (Tokyo, Japan). Natural
170 cellulosic fibers isolated from *Phyllostachys edulis* (moso bamboo) clum, namely
171 bamboo fibers, with a mixed particle size of 40 - 60 mesh were supplied by Anhui
172 Sentai WPC New Material Co. Ltd. (Anhui, China). Dopamine hydrochloride (assay ≥

98.5%), tris(hydroxymethyl aminomethane) (tris), sodium hydroxide (NaOH), ferrous dichloride tetrahydrate ($FeCl_2 \cdot 4H_2O$) and ferric chloride hexahydrate ($FeCl_3 \cdot 6H_2O$) were acquired from Aladdin (Beijing, China). All of the other analytical chemicals were sourced from Aladdin (Beijing, China).

2.2 Surface modification of bamboo fibers and fabrication of fiber-reinforced PBS biocomposites

Bamboo fibers were functionalized with Fe_3O_4-NPs and PPy based on PDA coupling, more details of the experimental procedure can be found in **Note S1**. The fabrication of fiber-reinforced PBS biocomposites was realized through a hot-pressing process, more details of the fabrication can be found in **Note S2**.

2.3 Characterization

Scanning electron microscopy (SEM, Hitachi SU8010) was carried out under an accelerating voltage of 10 kV to observe the surface morphologies of bamboo fibers as well as the fractured surface morphology of the biocomposites. An energy dispersive spectrometer (EDS) (JSM-7800F, Japan) was also used to detect C, O and Fe. All the samples were coated with an Au layer before observation.

Fourier transform infrared (FTIR, Nicolet, Madison, WI) spectroscopy was performed in the 500 - 4000 cm^{-1} range following a total of 40 scans to measure the surface functional groups of bamboo fibers. X-ray photoelectron spectroscopy (XPS, ESCALAB250) was performed with a monochromatic Al Kα ($h\upsilon$ = 1486.7 eV) X-ray source to examine the chemical/elemental states of bamboo fibers. X-ray diffraction (XRD, Bruker D8) measurements were performed in the 2θ range from 5° to 40° at a

testing speed of 2θ = 5°/min and the results were used to follow the crystallization of bamboo fibers.

A vibrating sample magnetometer (Squid VSM, Quantum Design, San Diego, CA, USA) was used to measure the magnetic properties of bamboo fibers in the range of -10,000 to 10,000 Oe. A four-point probe instrument (ST2253, Jingge Electronics (Suzhou) Co., Ltd., China) was used to measure the electrical conductivity of bamboo fibers at ambient temperature.

A universal testing machine (Kexin Instrument Equipment Co. Ltd., Changchun, China) was used to measure the tensile and flexural properties of the biocomposites at ambient temperature. A cantilever beam impact tester (Hebe Precision Testing Machine Co. Ltd., Chengde, China) was used to measure the impact resistance of the biocomposites at ambient temperature. More details of the measurements can be found in **Note S3**. A thermomechanical analyzer (DMA, NETZSCH, Selb, Germany) was used to measure the dynamic mechanical properties of the biocomposites (35 × 10 × 4 mm^3), at a temperature range between -60 and 40 °C (heating rate of 3 °C /min and scanning frequency of 1 Hz).

A vector network analyzer (Agilent, PNA-N5244A, USA) was used to evaluate the electromagnetic wave absorption and EMI performance of fiber-reinforced PBS biocomposites. The reflection loss (RL) value was measured on the basis of the arch method, in the frequency range between 2 and 18 GHz, by using 180 × 180 × 4 mm^3 samples. The EMI shielding effectiveness of the biocomposites was measured using a coaxial-line in the frequency range of 2 - 18 GHz. Samples were cut into cylinder (Φ_{out}

= 7.00 mm, Φ_{in} = 3.04 mm, thickness = 2 mm). The reflected power (R), transmitted power (T), and absorbed power (A) coefficients were obtained from the scattering parameters (S_{11} and S_{21}).

3. Results and discussion

3.1 Fiber Characterization

Fe_3O_4-NPs (used to introduce magnetic losses) and PPy (which introduce dielectric losses) were surface-coupled on bamboo fibers that were modified with PDA, **Fig. 1a**. In this process, PDA was used following the principle of adhesion in mussels. By contrast to the untreated bamboo fibers (**Fig. S2a**), the oxidative, self-polymerization of dopamine on the fibers formed a thin and rough surface (PDA coupled with BF, PDA-BF, **Fig. S2b**). The catechol moiety of PDA endowed coatings with ligand capabilities, *e.g.*, to directly immobilize Fe_3O_4-NPs through chelation and hence to build a magnetic-loss-activated interlayer on the surfaces of the PDA-treated fibers. EDS mapping images of MBF4 (**Fig. S2g - i**) indicated the distribution of C, O and Fe on the fibers, suggesting the successful dispersion and *in-situ* formation and deposition of Fe_3O_4-NPs on the surfaces of the fibers.

The unreacted Fe^{3+} in the interlayer served as an initiator of *in-situ* polymerization of pyrrole, *e.g.*, to establish a top layer in sandwich-like coatings. An apparent increase in coating thickness and roughness was observed with the addition of Fe_3O_4-NPs, as shown in **Fig. S2c**, **d**, **e**, **f** and **j**. The possible mechanism of co-deposition of PDA-Fe_3O_4-PPy on the fiber surface is shown schematically in **Fig. 1b**.

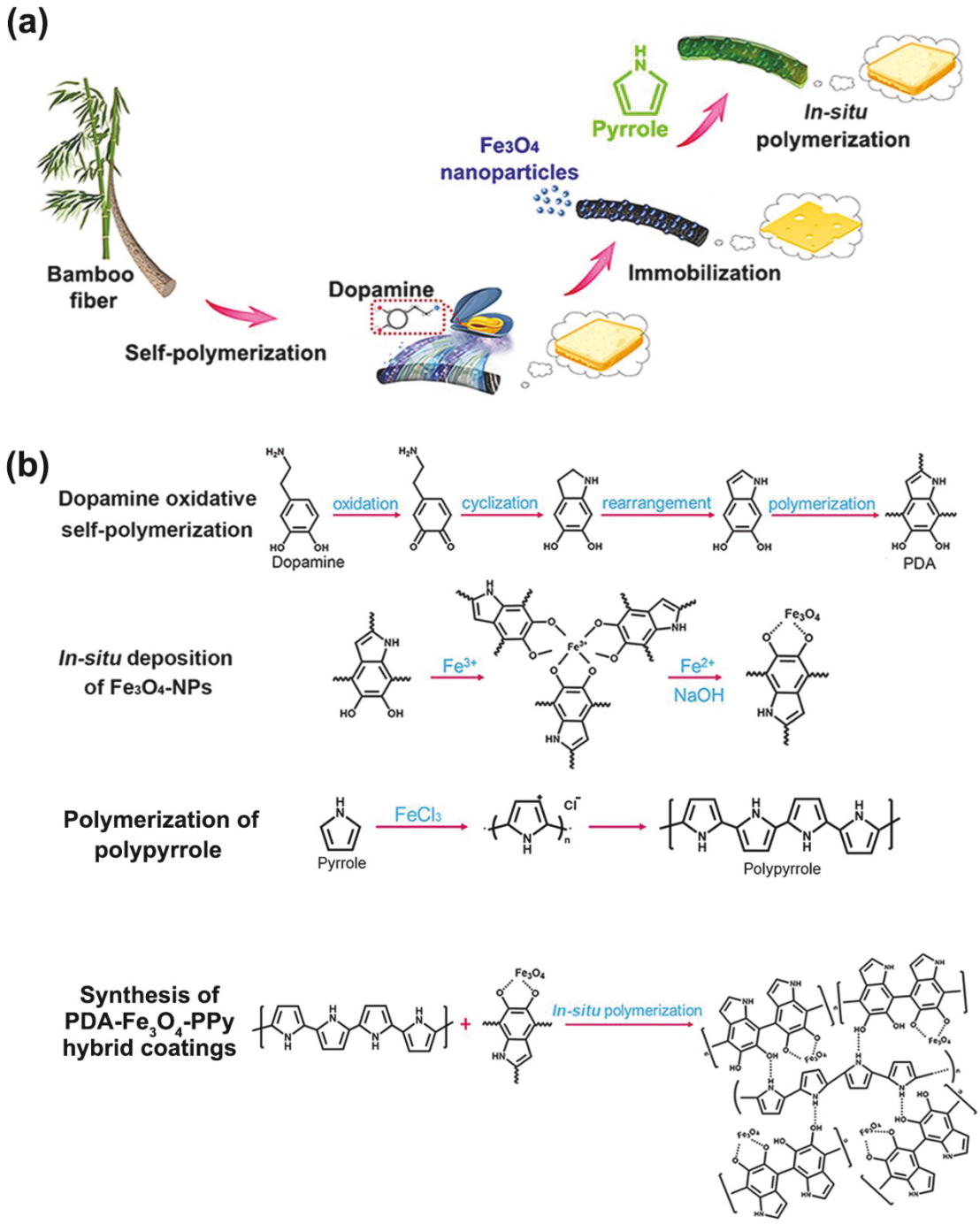

Fig. 1. (a) Schematic illustration of the *in-situ* interfacial synthesis of coatings on bamboo fibers; and **(b)** main chemical reactions involved in the synthesis of PDA-Fe_3O_4-PPy coatings

The FTIR spectra, together with XPS data and XRD analysis, demonstrate the successful surface modification of bamboo fibers. More detailed discussion of FTIR, XRD and XPS analysis of bamboo fibers can be found in reference to **Fig. S3, S4** and **S5**, respectively.

3.2 *Electromagnetic performance*

The magnetic performance of bamboo fibers was measured in the range of -10,000 to 10,000 Oe. As seen in **Fig. 2a**, the untreated fibers demonstrated the typical non-ferromagnetic property. After introducing Fe_3O_4-NPs on the fibers, a magnetic behavior was realized, with saturation magnetization (M_s) values of 2.1, 2.7, 3.4, 3.7 and 3.9 emμ/g for MBF1, MBF2, MBF3, MBF4, MBF5, respectively (**Table 1**). The significantly enhanced magnetism observed by the increased Fe_3O_4-NPs loading on the fibers is ascribed to the higher number density of metal particles (**Fig. S6**). Additionally, the coercivity (H_c) values of magnetic fibers increased with Fe_3O_4-NPs loading. The initial permeability (μ_i), was calculated according to equation 1(Zhan et al., 2018):

$$\mu_i = \left(\frac{{M_S}^2}{a\kappa H_c + b\lambda\xi}\right) \quad (1)$$

where a and b are the constants of materials, κ is the proportionality coefficient, λ is the elastic strain parameter, and ξ is the magnetostriction constant. According to the above equation, an enhanced permeability results from an increased M_s or decreased H_c. The H_c of the magnetic fibers was moderately enhanced with the addition of Fe_3O_4-NPs. However, the increasing amplitude of H_c, going from MBF1 to MBF5 (20.8%), is much lower than that of M_s (85.7%); hence, the latter factor was a dominant contribution to the permeability. Consequently, the enhanced magnetic effect is beneficial to improve the permeability of the prepared biocomposites, leading to an enhanced performance in microwave absorption.

Fig. 2b shows the changes in conductivity of the modified fibers with the increased Fe_3O_4-NPs loading. Obviously, the introduced modification endowed conductivity in

the modified fibers. The electrical conductivity of MBF1, MBF2, MBF3, MBF4, and MBF5 reached 0.311, 0.314, 0.317, 0.325 and 0.331 S/cm, respectively. The conductivity was increased with the addition of Fe_3O_4-NPs, which related to the increased deposition of Fe_3O_4-NPs and PPy. The as-prepared conductive fibers were pressed into a thin film, which let to LED lightning when connected with a wire in a current circuit (**Fig. 2c**), illustrating electron conductivity.

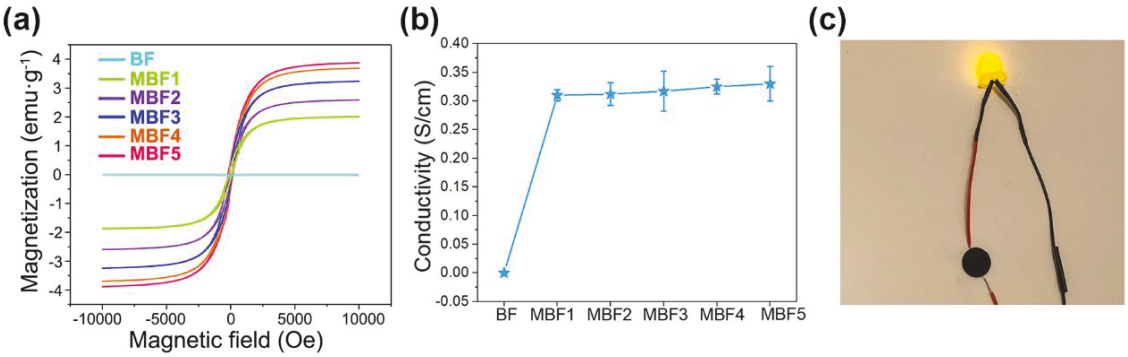

Fig. 2. (a) Magnetic hysteresis loops of untreated bamboo fibers (BF) and modified bamboo fibers (MBF1-MBF5); (b) changes in electrical conductivity of untreated bamboo fibers (BF) and modified bamboo fibers (MBF1-MBF5); and (c) digital photo of a circular thin film made with modified (MBF4) fibers as part of a circuit.

Table 1. Magnetic parameters of modified bamboo fibers (MBF1-MBF5).

Sample	Magnetic parameters	
	M_s (emμ/g)	H_c (Oe)
MBF1	2.1	143.7
MBF2	2.7	150.2
MBF3	3.4	161.4
MBF4	3.7	168.3
MBF5	3.9	173.6

3.3 Mechanical properties of fiber-reinforced PBS biocomposites

The static mechanical properties of PBS biocomposites reinforced with bamboo fibers were measured, including tensile strength and modulus, as well as flexural

strength and modulus along with impact strength, **Fig. 3**. Compared with PBS biocomposites produced with untreated fibers (BF), the tensile strength, tensile modulus, flexural strength and flexural modulus of the biocomposites containing PDA-treated fibers (PDA-BF) were significantly enhanced (by 18.3%, 8.1%, 7.1% and 5.5%, respectively). This is due to the enhanced interfacial interaction between PDA and PBS chains, which promoted stress transfer at the interface and supported external loading without interfacial phase separation. A more extensive improvement in tensile and flexural properties of the biocomposites was achieved with further introduction of Fe_3O_4-NPs and PPy on the PDA-modified bamboo fibers. This improvement likely resulted from the increased surface roughness provided by the chelated Fe_3O_4-NPs and PPy, which led to a greater specific surface area, and stronger interfacial adhesion (better interfacial interlocking between the fibers and the PBS matrix). When used in excess, Fe_3O_4-NPs agglomeration occurred; in such condition, the interfacial interaction between fibers and the PBS matrix was negatively affected (sample EMS5). Weakened interfacial adhesion resulted in a reduction of the static mechanical properties. Owing to the rigidity of PDA, Fe_3O_4-NPs and PPy, such biocomposite showed a reduced impact strength. An optimal performance was assigned to the EMS4 composite: compared to the biocomposites reinforced by the untreated fibers, the tensile strength, tensile modulus, flexural strength and flexural modulus were improved by 18, 38, 33 and 15%, respectively.

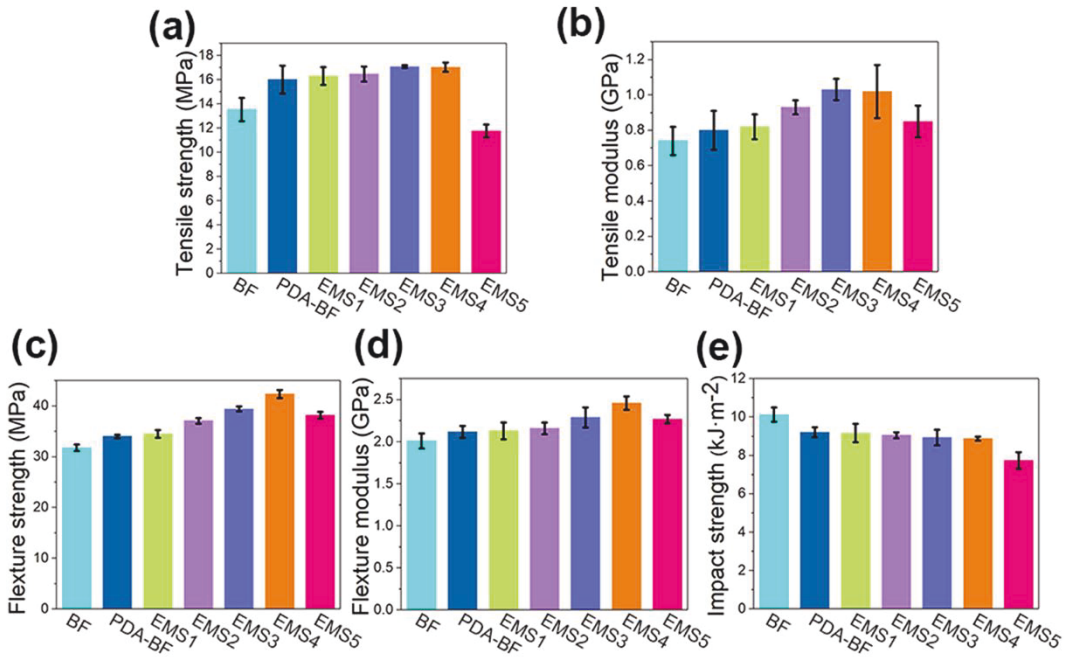

Fig. 3. Static mechanical properties of PBS-based biocomposites produced with untreated bamboo fibers (BF), PDA-treated fibers (PDA-BF) and PDA-treated fibers modified with Fe_3O_4-NPs and PPy at increased nanoparticle loading (EMS1-EMS5): Static mechanical properties of PBS-based biocomposites: (a) tensile strength; (b) tensile modulus; (c) flexural strength; (d) flexural modulus; and (e) impact strength.

3.4 Dynamic mechanical properties of fiber-reinforced PBS biocomposites

The dynamic mechanical properties of the fiber-reinforced PBS biocomposites, including storage modulus, the loss modulus and the loss factor are crucial to estimate the interfacial interaction of the as-obtained biocomposites. These properties were determined under oscillatory dynamic loading with an increased temperature, from -60 °C to 40 °C. Based on the thermoplastic characteristics of PBS, the storage modulus of all the PBS-based biocomposites was reduced with heating (**Fig. 4a**) (Chen, Cheng, Huang, Zou, & Zhao, 2017). Compared with the untreated fiber/PBS biocomposite (BF), an evident increase in storage modulus was observed in the case of those that reinforced by PDA-treated fibers (PDA-BF). Theoretically, the storage modulus tracks with the energy storage capacity and reflects the interfacial bonding in biocomposites;

these factors are principally connected with the stiffness of the material. The improved storage modulus of the biocomposites was attributed to the enhanced interfacial interaction between the PDA-treated fibers and the PBS matrix as well as the toughness of rigid PDA coupled on the fibers. As expected, the introduction of Fe_3O_4-NPs and PPy further improved the interfacial interaction of the as-prepared biocomposites, leading to a further increase in storage modulus. However, as discussed in the case of the static mechanical properties, an excess of Fe_3O_4-NPs (EMS5 sample) impaired the interfacial adhesion, resulting in a dramatical reduction in the storage modulus at the given temperature range.

Compared with the untreated fiber-reinforced PBS biocomposites (BF), an improved loss modulus was observed in PBS-based biocomposites containing PDA-modifed fibers treated with Fe_3O_4-NPs and PPy (EMS) (**Fig. 4b**). In addition, the loss modulus of the biocomposites moderately increased with the Fe_3O_4-NPs addition. This is due to the enhanced interfacial adhesion between the modified fibers and the PBS matrix, which caused more elastic energy conversion to thermal energy. Excess Fe_3O_4-NPs (EMS5) weakened the interfacial interaction of the biocomposites, which led to a decreased loss modulus. In general, the peak of the loss modulus, ascribed to the glass transition temperature (*Tg*), is a vital indicator of the interfacial adhesion of materials, which relates to the dissipation of energy in the biocomposites. Compared with the untreated fiber/PBS biocomposites (BF), a significant increase in *Tg* was noted for the PDA-treated fiber/PBS biocomposites (PDA-BF). The improved interfacial interaction given by PDA-treatment effectively restricted the movement of PBS chains, which

resulted in an increased PBS matric viscosity, thus leading to an enhanced *Tg* (Wang, Zhang, Zhang, Guo, & Wang, 2013). As expected, better interfacial interaction was achieved upon further treatment with Fe_3O_4-NPs and PPy (EMS1 to EMS4): the greater interfacial enhancement resulted in less energy dissipation and hinders the internal friction produced by the inner molecular motion, leading to a higher *Tg*.

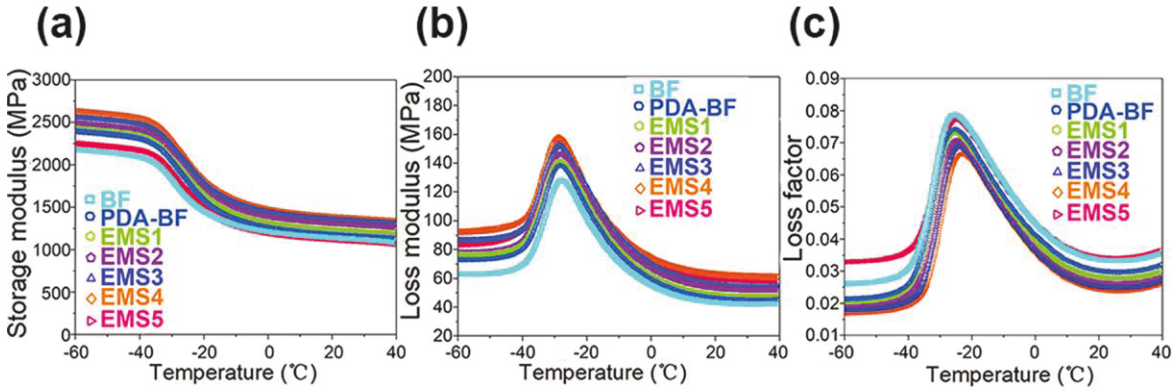

Fig. 4. DMA profiles of PBS-based biocomposites produced with untreated bamboo fibers (BF), PDA-treated fibers (PDA-BF) and PDA-treated fibers modified with Fe_3O_4-NPs and PPy at increased nanoparticle loading (EMS1-EMS5): (a) storage modulus; (b) loss modulus; and (c) loss factor.

The loss factor of the biocomposites is shown in **Fig. 4c**, which relates to the degree of intermolecular mobility in the biocomposites. Generally, the enhanced interfacial adhesion of materials contributes to a reduced macromolecular mobility, which results in a low loss factor (Kubát, Rigdahl, & Welander, 1990; Samal, Mohanty, & Nayak, 2009). PDA-treatment effectively enhanced the interfacial interaction between the fibers and the PBS matrix: the improved interfacial interaction against molecular slipping, led to a reduced loss factor. In addition, greater interfacial adhesion between the fibers and the PBS matrix was obtained with further treatment (Fe_3O_4-NPs and PPy) in the samples. This result indicates that a stronger interfacial adhesion was realized in

365 the as-obtained biocomposites, which contributed to the better stress transfer and load-
366 bearing ability. A weakened interfacial adhesion was generated from excess Fe_3O_4-NPs
367 (EMS5), leading to an increased loss factor. Overall, the optimal interfacial interaction
368 was achieved in the biocomposite denoted as EMS4.
369
370 *3.5 Morphology of fractured fiber-reinforced PBS biocomposites*
371 The morphology of the fractured area in samples with various fiber-reinforced PBS
372 biocomposites are shown in **Fig. 5**. An apparent phase separation between the untreated
373 fibers and the PBS matrix was observed. Abundant and irregular grooves and voids,
374 caused by the fiber pull-out, were distributed in the fractured surface**, Fig. 5a**$_1$. This is
375 due to polar fibers tending to aggregate in their natural state; furthermore, the interfacial
376 compatibility between the fibers and the nonpolar PBS matrix is poor; hence, weak
377 interfacial adhesion caused the fibers to easily pull out from the PBS matrix under load,
378 **Fig. 5a**. After PDA-treatment, the interfacial bonding between the modified fibers and
379 PBS matrix was significantly improved: the enhanced interfacial interaction efficiently
380 facilitated stress transfer and resisted external loading. In addition, the rough fiber
381 surface generated from the PDA treatment promoted tighter interfacial interlocking
382 between the fibers and the PBS matrix, effectively preventing fiber pull-out (**Fig. 5b**
383 and **Fig. 5b**$_1$). As seen in **Fig. 5c**, treatment with Fe_3O_4-NPs and PPy, produced better
384 interfacial bonding in the biocomposites, leading to a better stress transfer, which
385 effectively avoided interfacial damage. Distinctly, the interfacial interaction of the
386 biocomposites gradually improved with increased Fe_3O_4-NPs addition (**Fig. 5c**$_1$ **- 5c**$_4$),

which is due to the tougher interfacial interlocking created from the increased surface roughness. The corresponding elemental mapping of C, O and Fe in MBF4 are shown in **Fig. 5c$_5$ - 5c$_7$**, confirming the successful immobilization of Fe_3O_4-NPs on the fibers. However, when used in excess, Fe_3O_4-NPs aggregated, impairing interfacial adhesion and producing phase separation (EMS5, **Fig. 5c$_8$**).

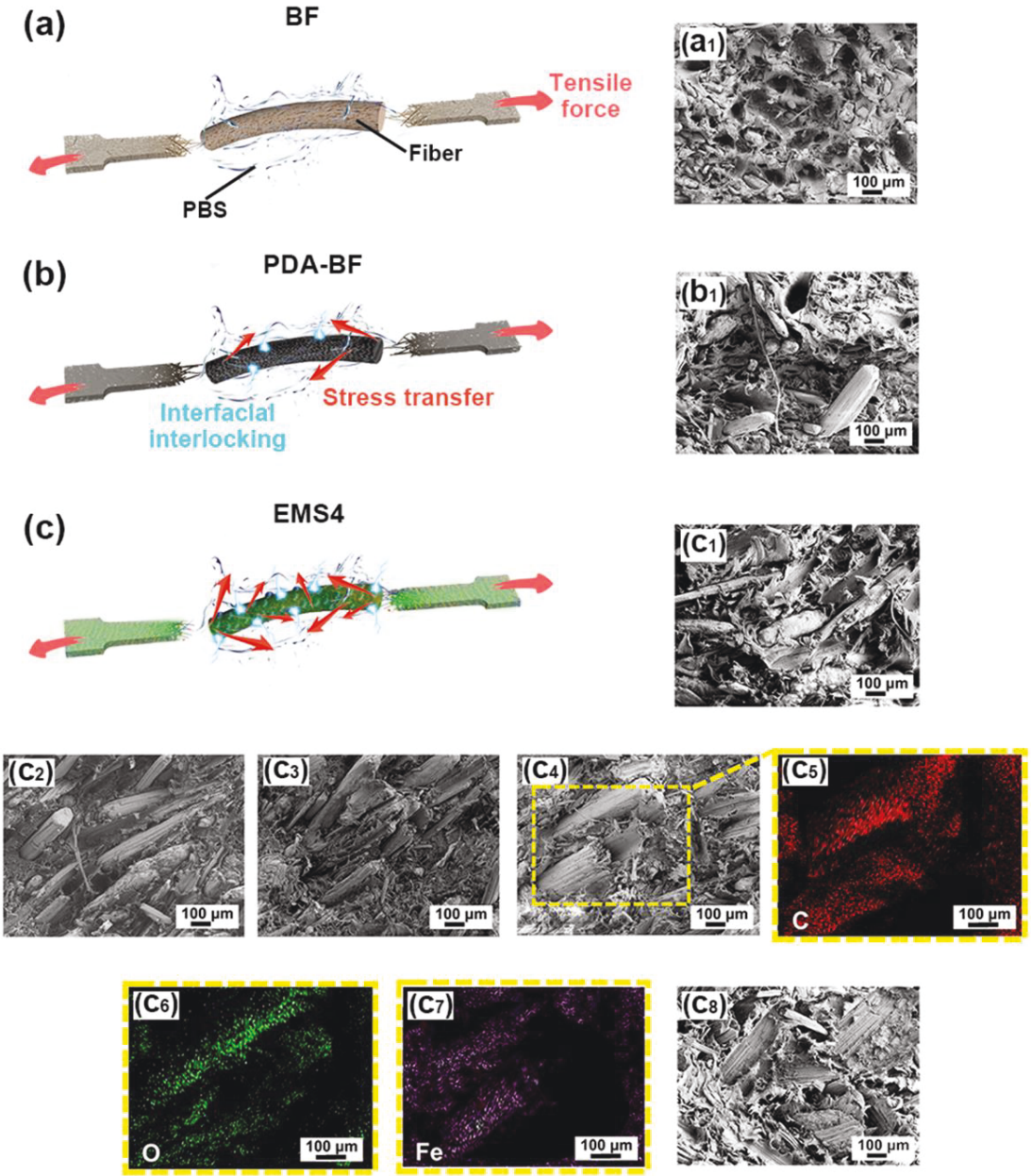

Fig. 5. (a) Schematic illustration of the interfacial adhesion of BF biocomposites. (a$_1$) SEM micrographs of BF biocomposites; (b) schematic illustration of the interfacial adhesion of PDA-BF biocomposites; (b$_1$) SEM micrographs of PDA-BF biocomposites; (c) schematic illustration of

interfacial adhesion of EMS4 biocomposites; (c_1) SEM micrographs of EMS1 biocomposites; (c_2) SEM micrographs of EMS2 biocomposites; (c_3) SEM micrographs of EMS3 biocomposites; (c_4) SEM micrographs of EMS4 biocomposites; (c_5) EDX elemental (C) mapping of EMS4; (c_6) EDX elemental (O) mapping of EMS4; (c_7) EDX elemental (Fe) mapping of EMS4; and (c_8) SEM micrographs of EMS5 biocomposites.

In brief, the mussel-inspired surface modification of bamboo fibers was shown as a promising route to obtain strong fiber-reinforced composites. The surface modification endowed functionality and improved interfacial interaction between the fibers and the polymer matrix.

3.6 Electromagnetic wave absorption of fiber-reinforced PBS biocomposites

The principle of electromagnetic absorption by the bamboo fiber-reinforced PBS biocomposites is schematically illustrated in **Fig. 6a**. In this system, functionalized bamboo fibers served as a 3D reticulated scaffold for multireflection and scattering; meanwhile, Fe_3O_4-NPs and PPy contributed to magnetic and dielectric losses, respectively, to optimize impedance matching. Besides, the heterogeneous interface of the modified fibers provided interfacial polarization. Hence, the mechanism of EMW attenuation by the PBS-based biocomposites was primarily attributed to the magnetic, dielectric and interfacial polarization losses, as well as the multireflection and scattering.

According to the proposed mechanism of EMW attenuation, impedance matching, is reflected by the relative dielectric constant ($\varepsilon_r = \varepsilon' - j\varepsilon''$) and the relative magnetic permeability ($\mu_r = \mu' - j\mu''$). Here, r presents the relative dielectric constant and the relative magnetic permeability play a key role in EMW attenuation. Based on the electromagnetic energy-conversion principle, the real part of the complex permittivity (ε') and permeability (μ') represent the storage capability of the electric and magnetic

energy, respectively, which reveal the extend of polarization and the generated dipoles in the absorber. The imaginary part of ε'' and μ'' refers to the loss capability of the electric and magnetic energy, respectively, produced from the dipole-orientation polarization under an electromagnetic field (Lü et al., 2015). As shown in **Fig. 6b** and **6c**, both ε' and ε'' were positively enhanced with Fe_3O_4-NPs loading, resulting from the better impedance matching as well as the stronger capability of electromagnetic attenuation generated from the improved conductivity of the reinforced fibers, which induced dielectric losses. The decreasing ε' was observed with frequency in all the PBS-based biocomposites (**Fig. 6b**), which was ascribed to the more extensive lagging of the dipole-polarization response with respect to the electric-field change at higher frequencies (Wang et al., 2012). Noteworthily, the dielectric loss tangent ($\tan \delta_\varepsilon = \varepsilon''/\varepsilon'$) was significative to estimate the EMW loss ability of the absorber (Quan et al., 2017). As the addition of Fe_3O_4-NPs increased, an increased $\tan \delta_\varepsilon$ was realized (**Fig. 6f**). This observation suggests that better EMW attenuation occurs in biocomposites with higher Fe_3O_4-NPs loading. In addition, the remanent Fe^{3+} in Fe_3O_4-NPs coatings therewith increased with the increased Fe_3O_4-NPs addition, inducing more PPy deposited on the fibers, which, synergistically resulted in the enhanced capability of converting EMW to energy in other forms. Moreover, the electron migrating and hopping produced from the interconnected conducive network also contributed to the greater dielectric loss.

Changes in μ' and μ'' of the fiber-reinforced PBS biocomposites are shown in **Fig. 6d** and **6e**. Interestingly, both μ' and μ'' of the biocomposites reinforced by the fibers treated with a high Fe_3O_4-NPs loading were distinctly higher. This result is attributed to the

444 better impedance matching generated from the addition of Fe_3O_4-NPs.

445 Further explanations can be rationalized following equations 2 and 3 (Yan et al., 2011):

446 $$\mu' = 1 + \left(\frac{M}{H}\right) cos\sigma \quad (2)$$

447 $$\mu'' = 1 + \left(\frac{M}{H}\right) sin\sigma \quad (3)$$

448 where M is the magnetization, H is the intensity of the external magnetic field, and σ is
449 the phase lag angle. The enhanced M_s of the functionalized bamboo fibers is the reason
450 for the improved permeability of biocomposites under the same external magnetic field.
451 Moreover, the magnetic loss tangent (tan $\delta_\mu = \mu''/\mu'$) also offered important evidence to
452 evaluate the capacity of EMW loss. Obviously, the tan δ_μ of the biocomposites increased
453 with Fe_3O_4-NPs addition (**Fig. 6g**), implying a greater EMW attenuation. Notably,
454 EMS4 and EMS5 revealed close values of tan δ_ε and tan δ_μ, indicating that impedance
455 matching was reached in the as obtained biocomposites.

456 RL is adopted to evaluate the EMW absorbing performance of the as-prepared fiber-
457 reinforced PBS biocomposites. As can be seen in **Fig. 6h**, Fe_3O_4-NPs loading made an
458 evident effect on the EMW absorbing capability of the as-obtained biocomposites. The
459 minimum RL value was reached in EMS1, which exhibited the poorest absorption
460 ability, -5.58 dB at 14.10 GHz. As expected, Fe_3O_4-NPs addition resulted in an
461 enhanced adsorption: -9.98 dB at 12.87 GHz, -13.45 dB at 11.91 GHz, -22.69 dB at
462 10.60 GHz and -25.06 dB at 9.45 GHz for EMS2, EMS3, EMS4 and EMS5,
463 respectively. Generally, the RL value under -5.0, -10.0, or -20.0 dB indicate more than
464 70, 90, or 99% EMW attenuation, suggesting an outstanding EMW absorbing capacity.
465

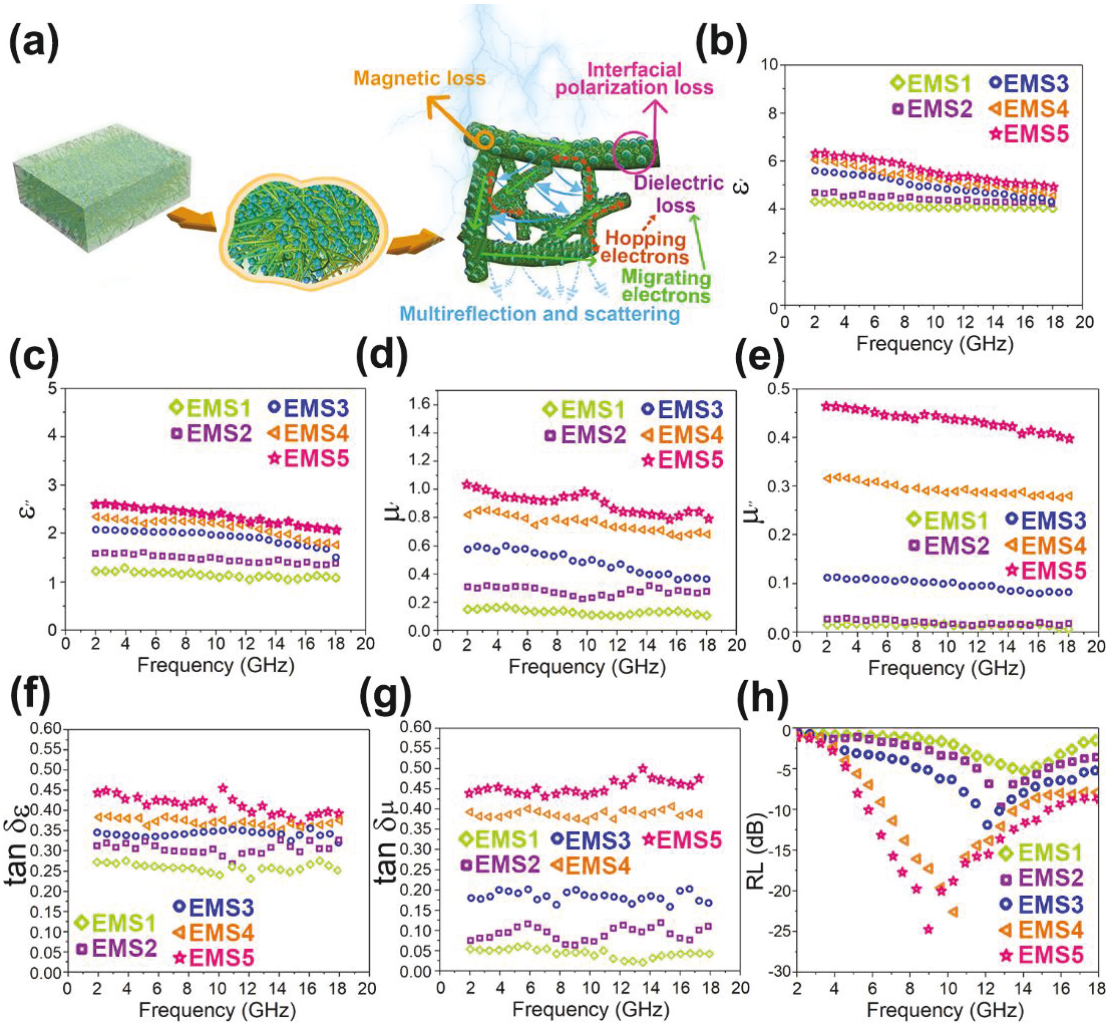

Fig. 6 (a) Electromagnetic absorption by PBS-based composites. (b)real part (ε') of complex permittivity; (c) imaginary part (ε'') of complex permittivity; (d) real part (μ') of complex permeability; (e) imaginary part (μ'') of complex permeability; (f) dielectric loss tangent (tan δ_ε); (g) magnetic loss tangent (tan δ_μ); and (h) reflection loss (RL) of fiber-reinforced PBS biocomposites.

3.7 EMI Performance of fiber-reinforced PBS biocomposites

The electromagnetic interference (EMI) shielding effectiveness (SE) of the biocomposites were investigated in the range of 2 - 18 GHz, which is widely used in communication applications including microwaves, cell phones, signal transmission and medical electronic devices. The total EMI shielding effectiveness (SE_T) is the sum of the reflection from the material surface (SE_R), the absorption of electromagnetic energy (SE_A), and the multiple internal reflections (SE_M). Transmissivity (T),

absorptivity (A), and reflectivity (R) can be calculated by following relations of the measured scattering parameters (S_{12} and S_{11}), which can be determined from: $T = |S_{21}|^2$, $R = |S_{11}|^2$, and A +R + T = 1. Normally, SE_M can be ignored when the value of SE_T is more than 15 dB. Therefore, the EMI SE calculation follows:

$$SE_R = -10\log(1 - R) = -10\log(1 - |S_{11}|^2) \quad (4)$$

$$SE_A = -10\log\left(\frac{T}{1-R}\right) = -10\log\left(\frac{|S_{21}|^2}{1-|S_{11}|^2}\right) \quad (5)$$

$$SE_T = SE_R + SE_A \quad (6)$$

Compared to the untreated bamboo, the EMI SE of fiber-reinforced PBS biocomposites (~2.1 dB) (**Fig. S7**, **Fig. 7)**, prepared with functionalized fibers, was dramatically increased. The values of SE, SE_A and SE_R increased with Fe_3O_4-NPs loading (**Fig. 7c - e**). Clearly, the major contributor to SE is attributed to SE_A, while the contribution of SE_R is negligible over the entire frequency region. As illustrated in **Fig. 7a**, the primarily contribution to EMI shielding performance is the combination of magnetic, dielectric and interfacial polarization losses. Accordingly, fibers with higher conductivity led to a conducting network within the PBS matrix, giving rise to a larger increase in electrical conductivity, inducing higher dielectric losses, which consequentially resulted in the improved SE and SE_A. Also, magnetic losses generated from Fe_3O_4-NPs contributed to the improved SE and SE_A. As discussed for the EMW absorbing properties, EMS4, and EMS5 revealed better impedance matching than the other biocomposites, which originated from an adequate Fe_3O_4-NPs and PPy loading on the fibers, producing an effective interaction for EMW attenuation. Meanwhile, the interfacial polarization created from the different dielectric properties of bamboo fibers,

PDA, Fe_3O_4-NPs, and PPy on the fibers were also beneficial in improving EMW shielding. The heterogeneous surface of the functionalized fibers efficaciously contributed to the attenuation of EMW. Moreover, the fiber-based scaffold efficiently induced multireflection and scattering to prolong EMW transmission routes for attenuation. Consequently, the proposed bamboo fiber/PBS biocomposites with EMI SE operated as a trap of microwaves escaping for secondary pollution. The EMI SE of EMS2, EMS3, EMS4, and EMS5 throughout the entire frequency range reached ~21.5 dB, ~28.4 dB, ~36.9 dB and ~39.8 dB, respectively, which fully satisfy the requirements of civil standards for practical use (~20 dB) (Singh et al., 2015). To achieve a good balance between ideal EMI SE and excellent mechanical properties, the optimal performance was assigned to EMS4. Notably, compared with other cellulose-based materials (see data from the literature in **Fig. 7b**), the introduced PBS-based biocomposites reinforced with functionalized bamboo fibers with desired EMI SE (~36.9 dB) represent an outstanding alternative for cellulose-based materials.

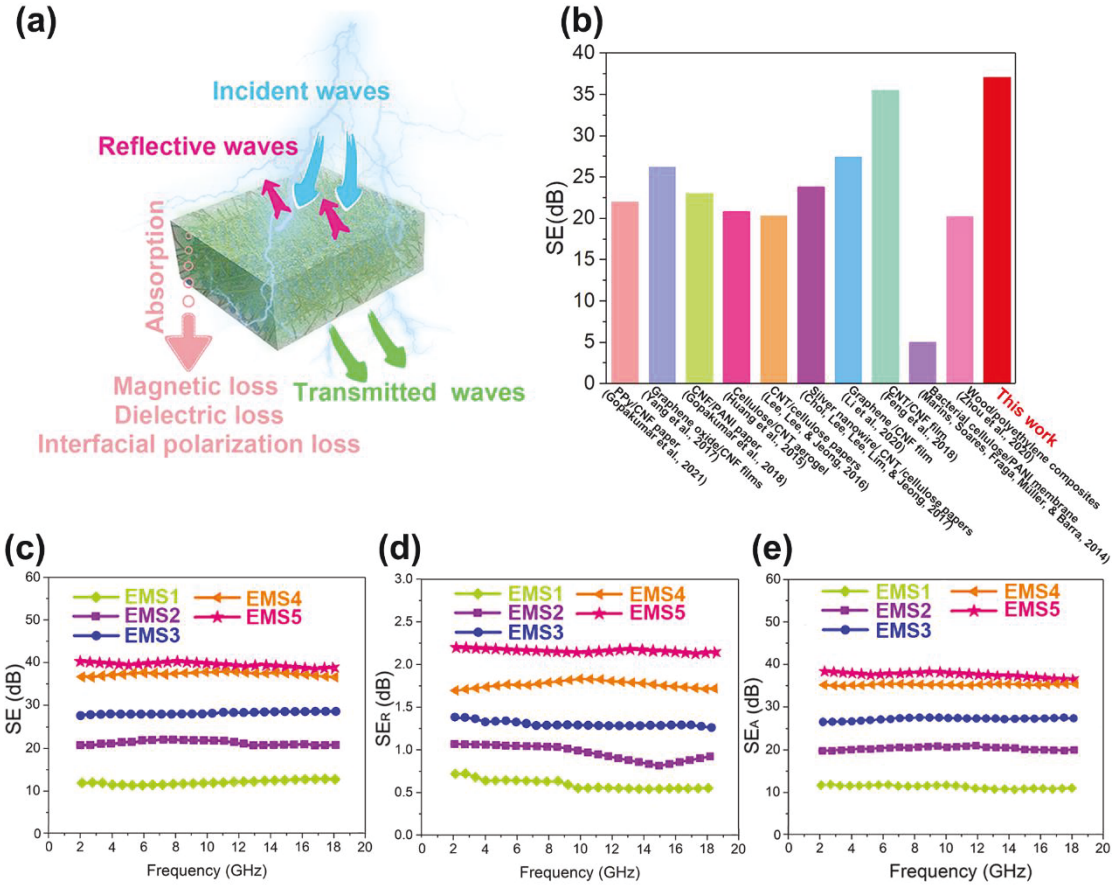

Fig. 7. (a) Scheme of primary EMI shielding processes; (b) comparison of EMI SE measured in this work relative to various cellulose-based materials; (c) SE of PBS-based biocomposite; (d) SE_R of PBS-based biocomposite; and (e) SE_A of PBS-based biocomposite.

4. Conclusions

Eco-friendly and lightweight bamboo fiber-reinforced PBS biocomposites are introduced for EMI shielding. A simple strategy is proposed for the proper distribution of magnetic loss-activated Fe_3O_4-NPs and dielectric loss-activated PPy on the surface of bamboo fibers. The functionalized fibers afforded distinct electric conductivity and magnetic behavior. An interconnected fiber network within PBS facilitates high absorption attenuation by a combination of multireflection, scattering, interfacial polarization, magnetic and dielectric losses. Meanwhile, satisfactory mechanical strength is realized due to the improved interfacial adhesion involving hybrid surface

coatings on the fibers. The tensile strength, tensile modulus, flexural strength and flexural modulus of the functionalized bamboo fiber-reinforced PBS biocomposites are higher than those unmodified composites. The balance between mechanical properties and desired EMI SE is achieved simultaneously. The characterization performed on the PBS biocomposites (structural, chemical, surface, thermo-mechanical and magnetic) is expected to guide future explorations aimed at designing high-performance bio-based absorption materials for EMW shielding and to reduce the impact of secondary pollution.

Credit authorship contribution statement

Gonghua Hong: Conceptualization, Methodology, Validation, Formal analysis, Software, Investigation, Data curation, Writing-Original Draft, Writing-Review & Editing. **Haitao Cheng**: Methodology. **Shuangbao Zhang**: Supervision, Project administration, Funding acquisition. **Orlando J. Rojas**: Supervision, Conceptualization, Writing-Review & Editing, Validation, Project administration, Funding acquisition.

Declaration of Competing Interest

The authors declare that they have no known competing financial interests or personal relationships that could have appeared to influence the work reported in this paper.

Acknowledgement

The financial support for this work was provided by the National Natural Science Foundation of China (32171707) and Beijing Natural Science Foundation (6202024). Orlando J. Rojas and Gonghua Hong acknowledge funding from the European Research Council (ERC) under the European Union's Horizon 2020 research and innovation program (ERC Advanced Grant Agreement No. 788489, "BioElCell"). Orlando J. Rojas is grateful to the Canada Excellence Research Chair initiative and the Canada Foundation for Innovation (CFI). Gonghua Hong is grateful to the funding from China Scholarship Council (CSC).

References

559 Chauhan, S. S., Abraham, M., & Choudhary, V. (2016). Superior EMI shielding
560 performance of thermally stable carbon nanofiber/poly(ether-ketone) composites in
561 26.5–40 GHz frequency range. *Journal of Materials Science*, 51(21), 9705-9715.
562 Chen, S., Cheng, L., Huang, H., Zou, F., & Zhao, H. P. (2017). Fabrication and
563 properties of poly(butylene succinate) biocomposites reinforced by waste silkworm silk
564 fabric. *Composites Part A: Applied Science and Manufacturing*, 95, 125-131.
565 Cheng, Y. L., Chen, Y. W., Wang, K., & Shie, M. Y. (2016). Enhanced adhesion and
566 differentiation of human mesenchymal stem cell inside apatite-
567 mineralized/poly(dopamine)-coated poly(ε-caprolactone) scaffolds by
568 stereolithography. *Journal of Materials Chemistry B*, 4(38), 6307-6315.
569 Choi, H. Y., Lee, T.-W., Lee, S.-E., Lim, J., & Jeong, Y. G. (2017). Silver
570 nanowire/carbon nanotube/cellulose hybrid papers for electrically conductive and
571 electromagnetic interference shielding elements. *Composites Science and Technology*,
572 150, 45-53.
573 Claramunt, J., Fernández-Carrasco, L. J., Ventura, H., & Ardanuy, M. (2016). Natural
574 fiber nonwoven reinforced cement composites as sustainable materials for building
575 envelopes. *Construction and Building Materials*, 115, 230-239.
576 Colaneri, N. F., & Schacklette, L. W. (1992). EMI shielding measurements of
577 conductive polymer blends. *IEEE Transactions on Instrumentation and Measurement*,
578 41(2), 291-297.
579 Dahy, H. (2019). Natural Fibre-Reinforced Polymer Composites (NFRP) Fabricated
580 from Lignocellulosic Fibres for Future Sustainable Architectural Applications, Case

581 Studies: Segmented-Shell Construction, Acoustic Panels, and Furniture. *Sensors*, 19(3),
582 738.
583 Feng, X., Qin, X., Liu, D., Huang, Z., Zhou, Y., Lan, W., . . . Qi, H. (2018). High
584 Electromagnetic Interference Shielding Effectiveness of Carbon Nanotube–Cellulose
585 Composite Films with Layered Structures. *Macromolecular Materials and Engineering*,
586 303(11), 1800377.
587 Geetha, S., Satheesh Kumar, K. K., Rao, C. R. K., Vijayan, M., & Trivedi, D. C. (2009).
588 EMI shielding: Methods and materials—A review. *Journal of Applied Polymer Science*,
589 112(4), 2073-2086.
590 Gopakumar, D. A., Pai, A. R., Pottathara, Y. B., Pasquini, D., Carlos de Morais, L.,
591 Luke, M., . . . Thomas, S. (2018). Cellulose Nanofiber-Based Polyaniline Flexible
592 Papers as Sustainable Microwave Absorbers in the X-Band. *ACS Applied Materials &*
593 *Interfaces*, 10(23), 20032-20043.
594 Gopakumar, D. A., Pai, A. R., Pottathara, Y. B., Pasquini, D., de Morais, L. C., Khalil
595 H.P.S, A., Nzihou, A., Thomas, S. (2021). Flexible papers derived from polypyrrole
596 deposited cellulose nanofibers for enhanced electromagnetic interference shielding in
597 gigahertz frequencies. *Journal of Applied Polymer Science*, 138(16), 50262.
598 Gopinath, R., Poopathi, R., & Saravanakumar, S. S. (2019). Characterization and
599 structural performance of hybrid fiber-reinforced composite deck panels. *Advanced*
600 *Composites and Hybrid Materials*, 2(1), 115-124.
601 Huang, H. D., Liu, C. Y., Zhou, D., Jiang, X., Zhong, G. J., Yan, D. X., & Li, Z. M.
602 (2015). Cellulose composite aerogel for highly efficient electromagnetic interference

603 shielding. *Journal of Materials Chemistry A*, 3(9), 4983-4991.
604 Huang, X. F., Pang, Y. C., Liu, Y. L., Zhou, Y., Wang, Z. K., & Hu, Q. L. (2016). Green
605 synthesis of silver nanoparticles with high antimicrobial activity and low cytotoxicity
606 using catechol-conjugated chitosan. *RSC Advances*, 6(69), 64357-64363.
607 He, Q., Liu, J., Liu, X., Li, G., Chen, D., Deng, P., & Liang, J. (2019). A promising
608 sensing platform toward dopamine using MnO2 nanowires/electro-reduced graphene
609 oxide composites. *Electrochimica Acta*, 296, 683-692.
610 He, Q. H., Li, D. M., He, Y. H., Zhang, Y. L., Shen, Z. Y., Zhu, L., . . . Chen, F. Y. (2017).
611 Microbeads preparation with reversed-phase microemulsion and ultraviolet light curing
612 for digital encoding suspension array. *RSC Advances*, 7(52), 32727-32730.
613 Ji, H., Zhao, R., Zhang, N., Jin, C., Lu, X., & Wang, C. (2018). Lightweight and flexible
614 electrospun polymer nanofiber/metal nanoparticle hybrid membrane for high-
615 performance electromagnetic interference shielding. *NPG Asia Materials*, 10(8), 749-
616 760.
617 Jiang, D., Murugadoss, V., Wang, Y., Lin, J., Ding, T., Wang, Z., . . . Guo, Z. (2019).
618 Electromagnetic Interference Shielding Polymers and Nanocomposites - A Review.
619 *Polymer Reviews*, 59(2), 280-337.
620 Ju, J., Kuang, T., Ke, X., Zeng, M., Chen, Z., Zhang, S., & Peng, X. (2020). Lightweight
621 multifunctional polypropylene/carbon nanotubes/carbon black nanocomposite foams
622 with segregated structure, ultralow percolation threshold and enhanced electromagnetic
623 interference shielding performance. *Composites Science and Technology*, 193, 108116.
624 Kalinke, C., Neumsteir, N. V., Aparecido, G. d. O., Ferraz, T. V. d. B., dos Santos, P. L.,

625 Janegitz, B. C., & Bonacin, J. A. (2020). Comparison of activation processes for 3D
626 printed PLA-graphene electrodes: electrochemical properties and application for
627 sensing of dopamine. *Analyst*, 145(4), 1207-1218.
628 Karteri, I., Altun, M., & Gunes, M. (2017). Electromagnetic interference shielding
629 performance and electromagnetic properties of wood-plastic nanocomposite with
630 graphene nanoplatelets. *Journal of Materials Science: Materials in Electronics*, 28(9),
631 6704-6711.
632 Khodiri, A. A., Al-Ashry, M. Y., & El-Shamy, A. G. (2020). Novel hybrid
633 nanocomposites based on polyvinyl alcohol/graphene/magnetite nanoparticles for high
634 electromagnetic shielding performance. *Journal of Alloys and Compounds*, 847,
635 156430.
636 Kraz, V., & Wallash, A. (2000). The effects of EMI from cell phones on GMR magnetic
637 recording heads and test equipment. Electrical Overstress/Electrostatic Discharge
638 Symposium Proceedings 2000 (IEEE Cat. No.00TH8476) (pp. 224-232).
639 Kubát, J., Rigdahl, M., & Welander, M. (1990). Characterization of interfacial
640 interactions in high density polyethylene filled with glass spheres using dynamic-
641 mechanical analysis. *Journal of Applied Polymer Science*, 39(7), 1527-1539.
642 Lecocq, H., Garois, N., Lhost, O., Girard, P. F., Cassagnau, P., & Serghei, A. (2020).
643 Polypropylene/carbon nanotubes composite materials with enhanced electromagnetic
644 interference shielding performance: Properties and modeling. *Composites Part B:*
645 *Engineering*, 189, 107866.
646 Lee, H., Scherer, N. F., & Messersmith, P. B. (2006). Single-molecule mechanics of

mussel adhesion. *Proceedings of the National Academy of Sciences*, 103(35), 12999.

Lee, T. W., Lee, S. E., & Jeong, Y. G. (2016). Carbon nanotube/cellulose papers with high performance in electric heating and electromagnetic interference shielding. *Composites Science and Technology*, 131, 77-87.

Li, L., Ma, Z., Xu, P., Zhou, B., Li, Q., Ma, J., . . . Liu, C. (2020). Flexible and alternant-layered cellulose nanofiber/graphene film with superior thermal conductivity and efficient electromagnetic interference shielding. *Composites Part A: Applied Science and Manufacturing*, 139, 106134.

Li, J. H., Ji, H. M., Xu, Y. F., Zhang, J. J., & Yan, Y. (2020). Three-dimensional graphene supported Fe3O4 coated by polypyrrole toward enhanced stability and microwave absorbing properties. *Journal of Materials Research and Technology*, 9(1), 762-772

Li, Y., Shen, B., Yi, D., Zhang, L., Zhai, W., Wei, X., & Zheng, W. (2017). The influence of gradient and sandwich configurations on the electromagnetic interference shielding performance of multilayered thermoplastic polyurethane/graphene composite foams. *Composites Science and Technology*, 138, 209-216.

Liang, C., Ruan, K., Zhang, Y., & Gu, J. (2020). Multifunctional Flexible Electromagnetic Interference Shielding Silver Nanowires/Cellulose Films with Excellent Thermal Management and Joule Heating Performances. *ACS Applied Materials & Interfaces*, 12(15), 18023-18031.

Lin, S. C., Ma, C. C. M., Hsiao, S. T., Wang, Y.S., Yang, C.Y., Liao, W. H., . . . Yang, R. B. (2016). Electromagnetic interference shielding performance of waterborne polyurethane composites filled with silver nanoparticles deposited on functionalized

669 graphene. *Applied Surface Science*, 385, 436-444.

670 Liu, C & Liao, X. P. (2020) Collagen Fiber/Fe3O4/Polypyrrole Nanocomposites for
671 Absorption-Type Electromagnetic Interference Shielding and Radar Stealth. *ACS*
672 *Applied Nano Materials*, 3(12), 11906-11915.

673 Liu, D., Song, J., Anderson, D. P., Chang, P. R., & Hua, Y. (2012). Bamboo fiber and
674 its reinforced composites: structure and properties. *Cellulose*, 19(5), 1449-1480.

675 Liu, Y., Wu, K., Lu, M., Nie, S., Chen, W., Jiao, E., . . . Lu, M. (2020). Vertically aligned
676 dopamine-reduced graphene oxide with high thermal conductivity for epoxy
677 nanocomposites. *Journal of Materials Science*, 55(21), 8917-8929.

678 Lü, Y., Wang, Y., Li, H., Lin, Y., Jiang, Z., Xie, Z., . . . Zheng, L. (2015). MOF-Derived
679 Porous Co/C Nanocomposites with Excellent Electromagnetic Wave Absorption
680 Properties. *ACS Applied Materials & Interfaces*, 7(24), 13604-13611.

681 Madhu, B. J., Gurusiddesh, M., Kiran, T., Shruthi, B., & Jayanna, H. S. (2016).
682 Structural, dielectric, ac conductivity and electromagnetic shielding properties of
683 polyaniline/Ni0.5Zn0.5Fe2O4 composites. Journal of *Materials Science: Materials in*
684 *Electronics*, 27(8), 7760-7766.

685 Marins, J. A., Soares, B. G., Fraga, M., Müller, D., & Barra, G. M. O. (2014). Self-
686 supported bacterial cellulose polyaniline conducting membrane as electromagnetic
687 interference shielding material: effect of the oxidizing agent. *Cellulose*, 21(3), 1409-
688 1418.

689 Markham, D. (1999). Shielding: quantifying the shielding requirements for portable
690 electronic design and providing new solutions by using a combination of materials and

691 design. *Materials & Design*, 21(1), 45-50.

692 Menon, A. V., Madras, G., & Bose, S. (2017). Magnetic Alloy-MWNT Heterostructure
693 as Efficient Electromagnetic Wave Suppressors in Soft Nanocomposites.
694 *ChemistrySelect*, 2(26), 7831-7844.

695 Mumtaz, S., Wang, L. S., Hussain, S. Z., Abdullah, M., Huma, Z., Iqbal, Z., . . . Hussain,
696 I. (2017). Dopamine coated Fe3O4 nanoparticles as enzyme mimics for the sensitive
697 detection of bacteria. *Chemical Communications*, 53(91), 12306-12308.

698 Nurul Fazita, M. R., Jayaraman, K., Bhattacharyya, D., Mohamad Haafiz, M. K.,
699 Saurabh, C. K., Hussin, M. H., & H.P.S., A. K. (2016). Green Composites Made of
700 Bamboo Fabric and Poly (Lactic) Acid for Packaging Applications—A Review.
701 *Materials*, 9(6), 435.

702 Ohlan, A., Singh, K., Chandra, A., & Dhawan, S. K. (2010). Microwave Absorption
703 Behavior of Core−Shell Structured Poly (3,4-Ethylenedioxy Thiophene)−Barium
704 Ferrite Nanocomposites. *ACS Applied Materials & Interfaces*, 2(3), 927-933.

705 Patterson, B. A., & Sodano, H. A. (2016). Enhanced Interfacial Strength and UV
706 Shielding of Aramid Fiber Composites through ZnO Nanoparticle Sizing. *ACS Applied*
707 *Materials & Interfaces*, 8(49), 33963-33971.

708 Quan, B., Liang, X., Xu, G., Cheng, Y., Zhang, Y., Liu, W., . . . Du, Y. (2017). A
709 permittivity regulating strategy to achieve high-performance electromagnetic wave
710 absorbers with compatibility of impedance matching and energy conservation. *New*
711 *Journal of Chemistry*, 41(3), 1259-1266.

712 Rengaswamy, K., Sakthivel, D. K., Muthukaruppan, A., Natesan, B., Venkatachalam,

S., & Kannaiyan, D. (2018). Electromagnetic interference (EMI) shielding performance of lightweight metal decorated carbon nanostructures dispersed in flexible polyvinylidene fluoride films. *New Journal of Chemistry*, 42(15), 12945-12953.

Sadjadi, S., Lazzara, G., Malmir, M., & Heravi, M. M. (2018). Pd nanoparticles immobilized on the poly-dopamine decorated halloysite nanotubes hybridized with N-doped porous carbon monolayer: A versatile catalyst for promoting Pd catalyzed reactions. *Journal of Catalysis*, 366, 245-257.

Samal, S. K., Mohanty, S., & Nayak, S. K. (2009). Polypropylene—Bamboo/Glass Fiber Hybrid Composites: Fabrication and Analysis of Mechanical, Morphological, Thermal, and Dynamic Mechanical Behavior. *Journal of Reinforced Plastics and Composites*, 28(22), 2729-2747.

Shen, B., Zhai, W., & Zheng, W. (2014). Ultrathin Flexible Graphene Film: An Excellent Thermal Conducting Material with Efficient EMI Shielding. *Advanced Functional Materials*, 24(28), 4542-4548.

Singh, A. K., Shishkin, A., Koppel, T., & Gupta, N. (2018). A review of porous lightweight composite materials for electromagnetic interference shielding. *Composites Part B: Engineering*, 149, 188-197.

Singh, B. P., Saket, D. K., Singh, A. P., Pati, S., Gupta, T. K., Singh, V. N., . . . Mathur, R. B. (2015). Microwave shielding properties of Co/Ni attached to single walled carbon nanotubes. *Journal of Materials Chemistry A*, 3(25), 13203-13209.

Tang, C. M., Tian, Y. H., & Hsu, S. H. (2015). Poly(vinyl alcohol) Nanocomposites Reinforced with Bamboo Charcoal Nanoparticles: Mineralization Behavior and

735 Characterization. *Materials*, 8(8), 4895-4911.

736 Wanasinghe, D., Aslani, F., Ma, G., & Habibi, D. (2020). Review of Polymer
737 Composites with Diverse Nanofillers for Electromagnetic Interference Shielding.
738 *Nanomaterials*, 10(3), 541.

739 Wang, H., Guo, H., Dai, Y., Geng, D., Han, Z., Li, D., . . . Zhang, Z. (2012). Optimal
740 electromagnetic-wave absorption by enhanced dipole polarization in Ni/C
741 nanocapsules. *Applied Physics Letters*, 101(8), 083116.

742 Wang, H., Zheng, K., Zhang, X., Wang, Y., Xiao, C., Chen, L., & Tian, X. (2018).
743 Separated poly(vinylidene fluoride)/carbon black composites containing magnetic
744 carbonyl iron particles for efficient electromagnetic interference shielding. *Materials*
745 *Research Express*, 5(12), 125304.

746 Wang, N., Zhang, Y., Chen, J., Zhang, J., & Fang, Q. (2017). Dopamine modified metal-
747 organic frameworks on anti-corrosion properties of waterborne epoxy coatings.
748 *Progress in Organic Coatings*, 109, 126-134.

749 Wang, W., Zhang, G., Zhang, W., Guo, W., & Wang, J. (2013). Processing and Thermal
750 Behaviors of Poly (Butylene Succinate) Blends with Highly-Filled Starch and Glycerol.
751 *Journal of Polymers and the Environment*, 21(1), 46-53.

752 Wang, Z., Zhao, H., Fan, L., Lin, J., Zhuang, P., Yuan, W. Z., . . . Tang, B. Z. (2011).
753 Chitosan rods reinforced by aligned multiwalled carbon nanotubes via magnetic-field-
754 assistant in situ precipitation. Carbohydrate Polymers, 84(3), 1126-1132.

755 Wen, B., Wang, X. X., Cao, W. Q., Shi, H. L., Lu, M. M., Wang, G., . . . Cao, M. S.
756 (2014). Reduced graphene oxides: the thinnest and most lightweight materials with

757 highly efficient microwave attenuation performances of the carbon world. *Nanoscale*,
758 6(11), 5754-5761.
759 Wu, J., Chen, J., Zhao, Y., Liu, W., & Zhang, W. (2016). Effect of electrophoretic
760 condition on the electromagnetic interference shielding performance of reduced
761 graphene oxide-carbon fiber/epoxy resin composites. *Composites Part B: Engineering*,
762 105, 167-175.
763 Xu, C., Shamey, R., & Hinks, D. (2010). Activated peroxide bleaching of regenerated
764 bamboo fiber using a butyrolactam-based cationic bleach activator. *Cellulose*, 17(2),
765 339-347.
766 Yan, S. J., Zhen, L., Xu, C. Y., Jiang, J. T., Shao, W. Z., & Tang, J. K. (2011). Synthesis,
767 characterization and electromagnetic properties of Fe1−xCox alloy flower-like
768 microparticles. *Journal of Magnetism and Magnetic Material*s, 323(5), 515-520.
769 Yan, X., Zhu, X., Ruan, Y., Xing, T., Chen, G., & Zhou, C. (2020). Biomimetic,
770 dopamine-modified superhydrophobic cotton fabric for oil–water separation. *Cellulose*,
771 27(13), 7873-7885.
772 Yan, Y., Zheng, Z., Deng, C., Li, Y., Zhang, X., & Yang, P. (2013). Hydrophilic
773 Polydopamine-Coated Graphene for Metal Ion Immobilization as a Novel Immobilized
774 Metal Ion Affinity Chromatography Platform for Phosphoproteome Analysis.
775 *Analytical Chemistry*, 85(18), 8483-8487.
776 Yang, W., Zhao, Z., Wu, K., Huang, R., Liu, T., Jiang, H., . . . Fu, Q. (2017). Ultrathin
777 flexible reduced graphene oxide/cellulose nanofiber composite films with strongly
778 anisotropic thermal conductivity and efficient electromagnetic interference shielding.

Journal of Materials Chemistry C, 5(15), 3748-3756.

Ye, Q., Zhou, F., & Liu, W. (2011). Bioinspired catecholic chemistry for surface modification. *Chemical Society Reviews*, 40(7), 4244-4258.

Yu, Z., Dai, T., Yuan, S., Zou, H., & Liu, P. (2020). Electromagnetic Interference Shielding Performance of Anisotropic Polyimide/Graphene Composite Aerogels. *ACS Applied Materials & Interfaces*, 12(27), 30990-31001.

Zeng, G., Ye, Z., He, Y., Yang, X., Ma, J., Shi, H., & Feng, Z. (2017). Application of dopamine-modified halloysite nanotubes/PVDF blend membranes for direct dyes removal from wastewater. *Chemical Engineering Journal*, 323, 572-583.

Zeng, Z., Chen, M., Pei, Y., Seyed Shahabadi, S. I., Che, B., Wang, P., & Lu, X. (2017). Ultralight and Flexible Polyurethane/Silver Nanowire Nanocomposites with Unidirectional Pores for Highly Effective Electromagnetic Shielding. *ACS Applied Materials & Interfaces*, 9(37), 32211-32219.

Zhan, Y., Long, Z., Wan, X., Zhang, J., He, S., & He, Y. (2018). 3D carbon fiber mats/nano-Fe3O4 hybrid material with high electromagnetic shielding performance. *Applied Surface Science*, 444, 710-720.

Zhang, C., He, Y., Zhan, Y., Zhang, L., Shi, H., & Xu, Z. (2017). Poly(dopamine) assisted epoxy functionalization of hexagonal boron nitride for enhancement of epoxy resin anticorrosion performance. *Polymers for Advanced Technologies*, 28(2), 214-221.

Zhang, M., Zhang, P., Wang, Q., Li, L., Dong, S., Liu, J., & Rao, W. (2019). Stretchable liquid metal electromagnetic interference shielding coating materials with superior effectiveness. *Journal of Materials Chemistry C*, 7(33), 10331-10337.

Zhao, H. B., Fu, Z. B., Chen, H. B., Zhong, M. L., & Wang, C.-Y. (2016). Excellent Electromagnetic Absorption Capability of Ni/Carbon Based Conductive and Magnetic Foams Synthesized via a Green One Pot Route. *ACS Applied Materials & Interfaces*, 8(2), 1468-1477.

Zhou, H., Xiao, Z., Wang, Y., Hao, X., Xie, Y., Song, Y., . . . Wang, Q. (2020). Conductive and fire-retardant wood/polyethylene composites based on a continuous honeycomb-like nanoscale carbon black network. *Construction and Building Materials*, 233, 117369.

Supporting information

Polydopamine-treated hierarchical cellulosic fibers as versatile reinforcement of polybutylene succinate biocomposites for electromagnetic shielding

Gonghua Hong [a,b,c], Haitao Cheng [e], Shuangbao Zhang [a,b,*], and Orlando J. Rojas [c,d,*]

[a] Beijing Key Laboratory of Wood Science and Engineering, Beijing Forestry University, Beijing 100083, China
[b] MOE Key Laboratory of Wooden Material Science and Application, Beijing Forestry University, Beijing 100083, China
[c] Department of Bioproducts and Biosystems, Aalto University, Vuorimiehentie 1, Espoo, P.O. Box 16300, FI-00076 Aalto, Finland
[d] Bioproducts Institute, Department of Chemical & Biological Engineering, Department of Chemistry, and Department of Wood Science, The University of British Columbia, 2360 East Mall, Vancouver, BC V6T, 1Z3, Canada
[e] Bamboo and Rattan Science and Technology Key Laboratory of the State Forestry Administration, International Centre for Bamboo and Rattan, Beijing 100102, PR China

[*] Corresponding authors:
Shuangbao Zhang: shuangbaozhang@163.com
Orlando J. Rojas: orlando.rojas@ubc.ca

Note S1. *Surface modification of bamboo fibers*

Bamboo fibers were repeatedly washed with deionized water and anhydrous ethanol to remove surface impurities. The fibers obtained after drying at 80 ± 2 °C (24 h) are therein termed "BF". PDA functionalization of the fibers was achieved by adding 2.0 mg/mL dopamine to 5g BF in a 100 mL tris buffer solution (pH 8.5), stirred at room temperature (~23 °C) for 24 h. After repeatedly washing with deionized water, the sample was dried at 80 ± 2 °C for 24 h and the PDA-modified fibers were labelled as PDA-BF. Fe_3O_4-NPs were formed and attached to the surfaces of the fibers by mixing 5g PDA-BF in a 500-mL NaOH solution (0.5 mol/L) followed by addition of $FeCl_2 \cdot 4H_2O$ at given concentrations (0.1, 0.2, 0.3, 0.4 and 0.5 mol/L) and quantitative amounts of $FeCl_3 \cdot 6H_2O$ ($FeCl_2 \cdot 4H_2O$: $FeCl_3 \cdot 6H_2O$=1:2.7) under stirring at 80 °C for 12h. The obtained hybrid fibers were repeatedly washed with deionized water, and designated as F1, F2, F3, F4, and F5, depending on the Fe_3O_4 nanoparticle loading. Finally, a top layer of PPy was deposited through vapor-phase polymerization. For this, 5 g of (PDA@Fe_3O_4-NPs)-treated fibers (F1, F2, F3, F4, and F5) were placed in a dish besides another dish containing 2 mL pyrrole monomer, both placed in a sealed container at 50 °C for 24h. After washing with ethanol and deionized water, the modified bamboo fibers were dried at 80 ± 2 °C for 24 h, and designated as MBF1, MBF2, MBF3, MBF4, and MBF5, corresponding to F1, F2, F3, F4, and F5, respectively.

Note S2. *Fabrication of fiber-reinforced PBS biocomposites*

The prepared fibers (BF, PDA-BF, MBF1, MBF2, MBF3, MBF4, and MBF5) were dried at 80 ± 2 °C until constant weight. The modified fibers and PBS were mixed for 15 min at a mass

ratio of 2:3 in a high-speed blender (SHR-A, Zhengzhou Jinhe Equipment Manufacturing Co. LTD, China), operating at room temperature. They were then melt-blended in a co-rotating twin-screw extruder (KESUN KS-20, Kunshan, China) at a processing temperature ranging from 135 °C to 145 °C. The fiber-reinforced PBS biocomposites were prepared with a steel model (270 × 270 × 4 mm^3) through hot-pressing (4 MPa for 6 min at 145 °C) (SYSMEN-II, China Academy of Forestry, Beijing, China) and pressing (4 MPa for 6 min at room temperature) (QD, Shenzhen Jemai Precision Automation Co. LTD, China), the image of the fiber-reinforced PBS biocomposite can be seen in **Fig.S1**. The obtained fiber-reinforced PBS biocomposites (electromagnetic shields) were designated as BF, PDA-BF, EMS1, EMS2, EMS3, EMS4 and EMS5.

Note S3. *Mechanical properties*

A universal testing machine (Kexin Instrument Equipment Co. Ltd., Changchun, China) was used to measure the tensile and flexural properties of the biocomposites at ambient temperature. Samples with dumbbell-shape were custom-made for tensile tests, which followed the ASTM D638-03 (2003) standard. The flexural properties were determined according to the ASTM D790-03 (2003) standard using 100 × 30 × 4 mm^3 samples under a three-point bending test (span of 64 mm and crosshead speed of 2 mm/min). A cantilever beam impact tester (Hebe Precision Testing Machine Co. Ltd., Chengde, China) was used to measure the impact resistance of the biocomposites at ambient temperature according to ASTM D256-03 (2003) using 80 × 30 × 4 mm^3 samples. The average values of tensile, flexural and impact properties for each sample were calculated from at least five samples.

Note S4. *Thermal behavior*

A Mettler Toledo TGA/SDTA 851E thermal analysis was used to measure the weight loss of bamboo fibers in an nitrogen atmosphere at a temperature range between 30°C and 800 °C with the rate of 10 °C/min.

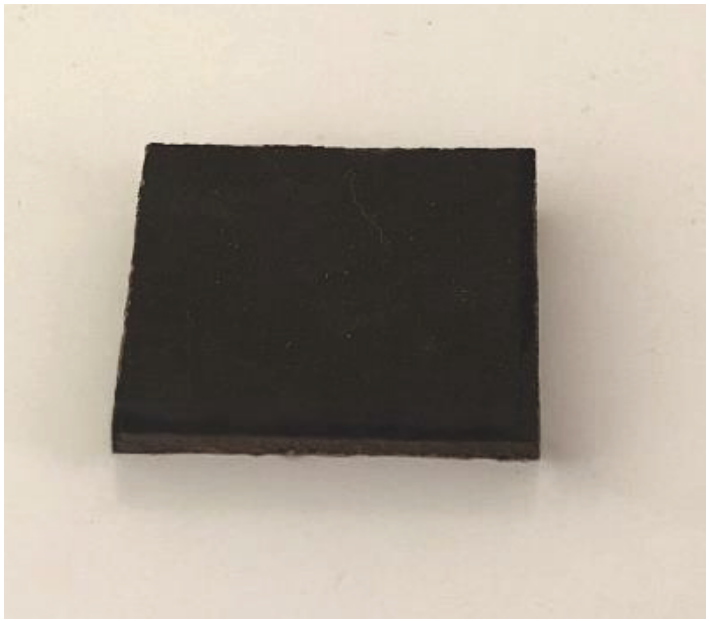

Fig. S1. Image of bamboo fiber-reinforced PBS biocomposite.

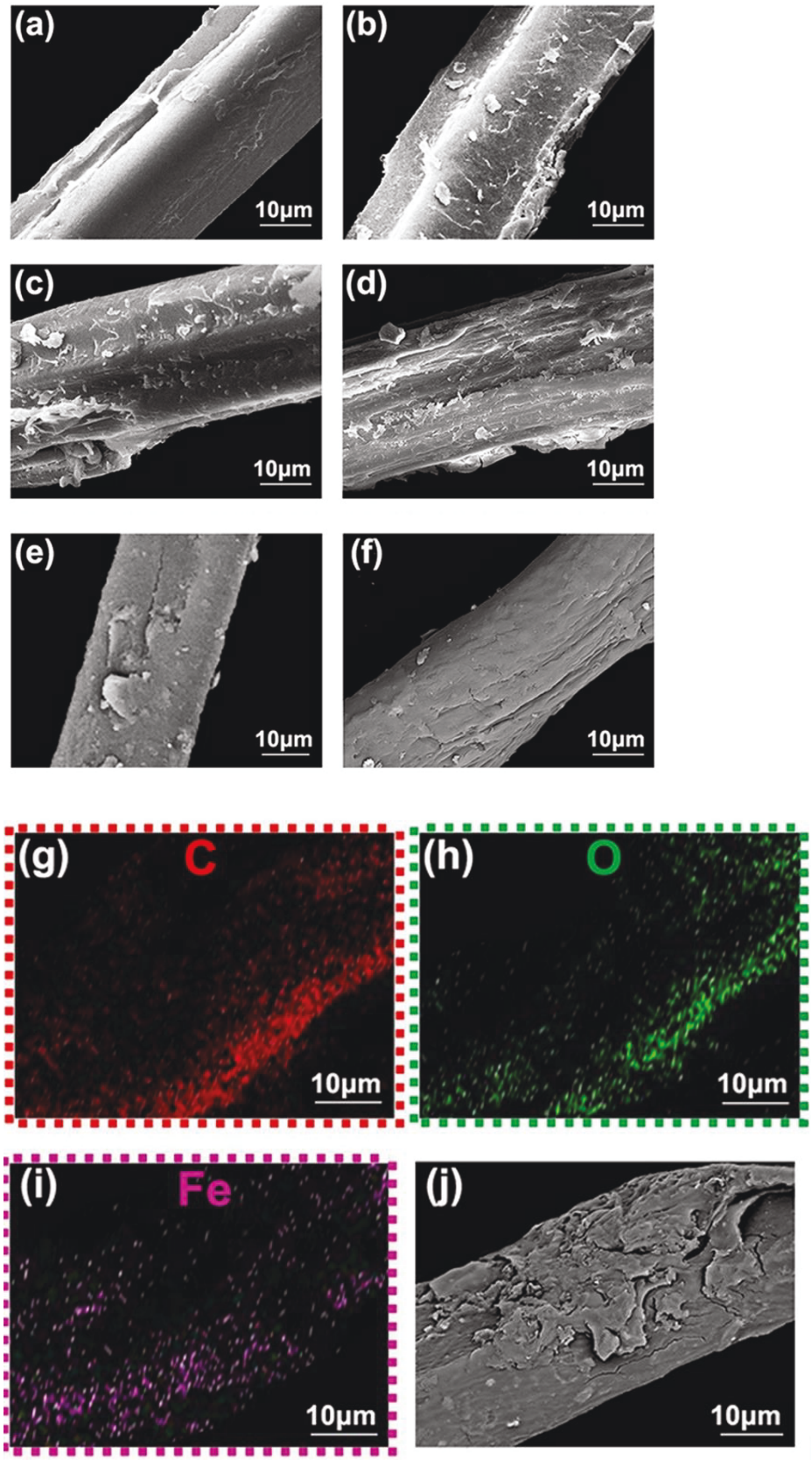

Fig. S2. SEM images of **(a)** BF; **(b)** PDA-BF; **(c)** MBF1; **(d)** MBF2; **(e)** MBF3; **(f)** MBF4; **(g)** EDX elemental (C) mapping of MBF4; **(h)** EDX elemental (O) mapping of MBF4; **(i)** EDX elemental (Fe) mapping of MBF4; and **(j)** MBF5.

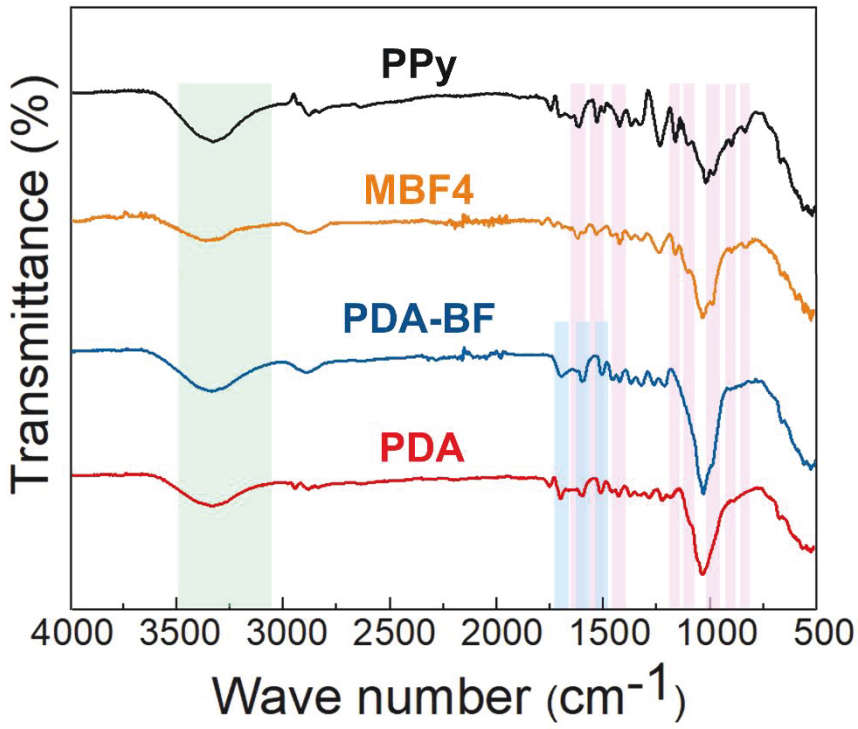

Fig. S3. FTIR spectrum of PDA, PPy, PDA-BF and MBF4.

The FTIR spectra of PDA and PDA-BF (**Fig. S3**) presented a broad band near 3400 cm^{-1}, which is assigned to N–H/O–H stretching vibrations in the PDA coatings. The IR absorption band located at *ca*. 1595, 1720 and 1500 cm^{-1} were assigned to C=C, C=O resonance vibrations of the aromatic ring and N–H bending vibrations, respectively, which are the characteristic of PDA, indicating the successful deposition of PDA on the bamboo fibers (J. Jiang, Zhu, Zhu, Zhu, & Xu, 2011). The IR absorption bands located at *ca*. 1450, 1534 and 3455 cm^{-1} of PPy were assigned to C−N, C−C and N−H stretching vibrations of the pyrrole ring, respectively (Zhong, Gao, Xue, & Wang, 2015). The bands near 896 and 1105 and 1630 cm^{-1} were mostly assigned to the C−H out-of-plane deformation, N−H in-plane deformation and PPy ring vibrations, respectively (X.-G. Li, Li, Huang, Liao, & Lu, 2010). The band around 1170 cm^{-1} was related to the doping state of PPy. Additionally, the band near 901/795

cm^{-1} was due to the =C−H out-of-plane deformation vibration, demonstrating the polymerization of pyrrole (Zhong et al., 2015). The spectrum of MBF4 showed a great match with PPy, revealing the existence of PPy on the surfaces of the as-treated fibers. However, the FTIR spectra was insensitive to the inorganic component, *i.e.*, the chemical changes in Fe_3O_4-treated bamboo fibers were difficult to detect by FTIR and were further examined by XPS and XRD.

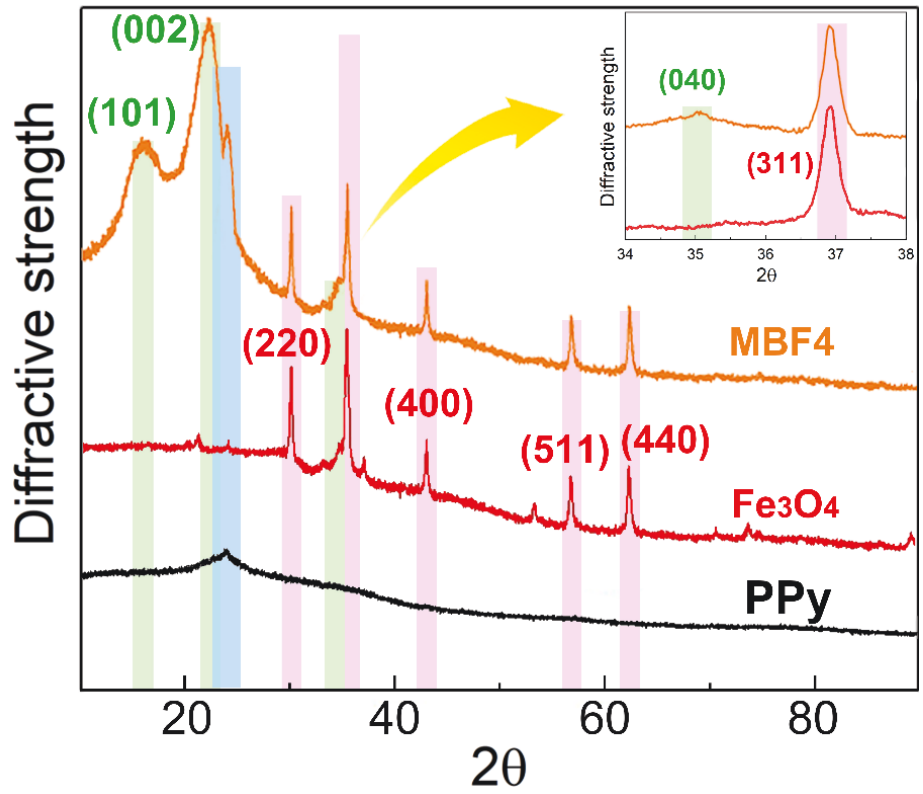

Fig. S4. XRD patterns of PPy, Fe_3O_4 and MBF4.

The phase composition and crystalline structure of the fibers were evaluated by XRD, **Fig. S4**. For bamboo fibers, the diffraction peaks at 17° (101), 22.5° (002) and 35° (040) are typical of the crystal structure of native cellulose I (Yao, Wang, Li, & Duan, 2017). After surface modification, distinct diffraction peaks at 30.1° (220), 36.8° (311), 43.3° (400), 57.2°

(551) and 62.7° (440) were observed, which were a manifestation of the Fe_3O_4 crystalline phase.(M. Liu, Chen, Hu, Wu, & Wang, 2011; H. Wu, Gao, Zhou, Zhang, & Guo, 2012). The amorphous diffraction peak around 2θ = 23° corresponded to the characteristic peak of PPy (Luo & Gao, 2014).

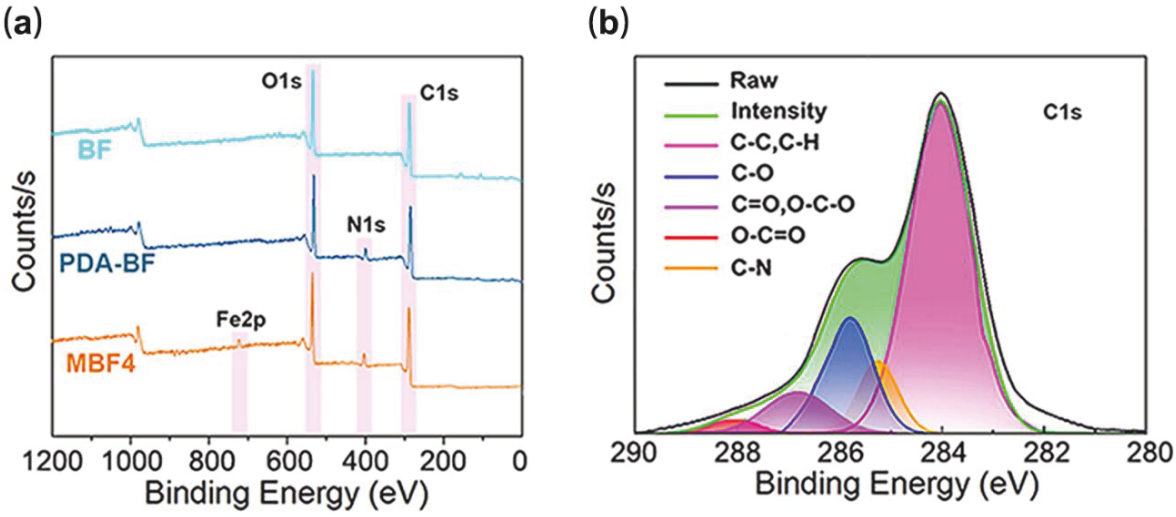

Fig. S5. (a) XPS wide-scan of BF, PDA-BF and MBF4 and **(b)** C1s core-level spectra of PDA-BF.

Table S1. Surface element characterization of BF, PDA-BF and MBF4.

Sample	Composition (At. %)				Atom ratio
	C	O	N	Fe	N/C
BF	73.1	26.9	-	-	-
PDA-BF	70.2	23.7	6.1	-	0.09
MBF4	76.9	13.7	8.3	1.1	0.11

XPS analyses further confirmed the coating on the fibers. The characteristic peaks at binding energies of 285 and 530 eV for C1s and O1s, respectively, were assigned to the main elements of lignocellulose, **Fig. S5 (a)** (W. Liu, Xie, & Qiu, 2016). As expected, an additional N1s peak (6.1% N atom content) appeared in the spectra of PDA-BF at 400 eV, suggesting the successful coupling of PDA on the fiber surface. The C1s high resolution spectrum of PDA-BF consisted of five peaks at 283.9, 285.2, 285.5, 285.8 and 287.6 eV, corresponding to C–C/C–H, C–O, C–N, C=O/O–C–O and O–C=O, respectively (G. Xu, Wang, Liu, & Wu, 2013). Also, a new peak emerged in the C1s high resolution spectra of PDA-BF, at 285.5 eV for C-N, which further confirmed the successful reaction between bamboo fibers and PDA (**Fig. S5b**). For MBF4, the atom content (at.%) of C and N were higher than those in PDA-BF, while the at.% of O was much lower compared to that in PDA-BF; these changes are likely related to the presence of PPy. In addition, the increasing N/C atom ratio (0.11) in MBF4 further verified the *in-situ* polymerization of pyrrole on the fibers (**Table S1**). A new Fe2p peak at a binding energy of 711 eV was observed in the MBF4 spectrum, indicating the existence of Fe_3O_4-NPs.

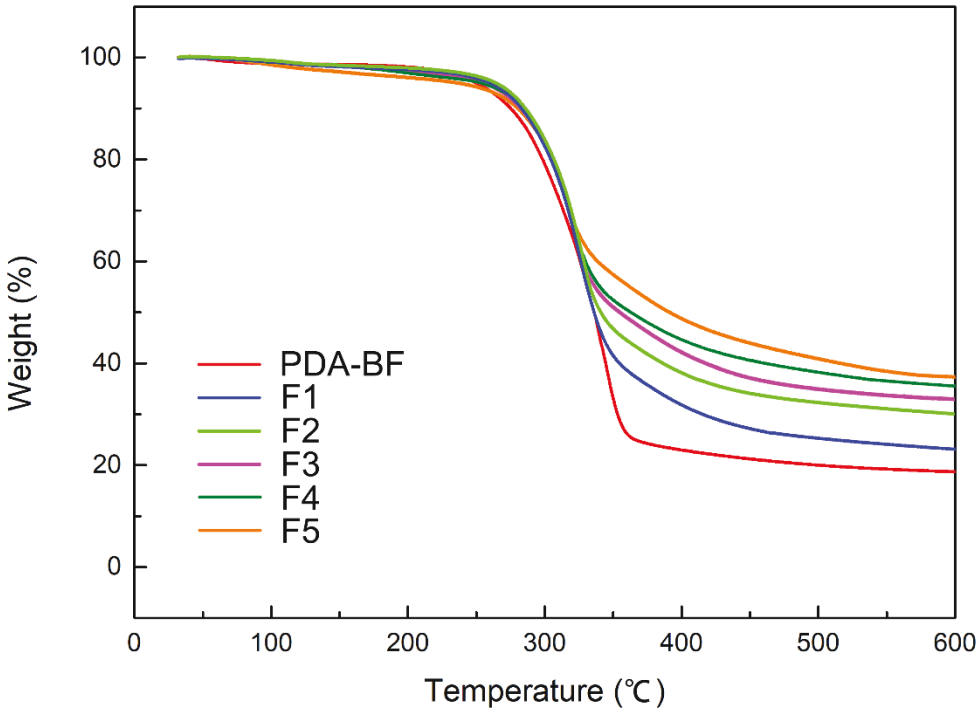

Fig. S6. TGA curves of bamboo fibers.

In order to eliminate the measuring error as much as possible, and obatin the most accurate results, PDA-treated bamboo fibers were used as a whole to calculate the Fe_3O_4-NPs content after (PDA@Fe_3O_4-NPs)-treatment. As shown in **Fig. S6**, all of the bamboo fibers were stable up to about 250 °C. As the temperature continued to rise, the residual mass of fibers reamined stable beyond 550 °C, which indiacted the end of the thermo-decomposition process. PDA-treated bamboo fibers (PDA-BF) included a 20.4 wt% residue at 600 °C, whereas the residual mass for F1, F2, F3, F4 and F5 were 26.8, 31.6, 35.8, 39.3 and 43.0 wt%, respectively. Fe_3O_4-NPs were unusually stable below 800 °C under a nitrogen atmosphere (Khandanlou, Ahmad, Shameli, Saki, & Kalantari, 2014). The increased residue mass assume to be due to Fe_3O_4-NPs. Therefore, the content of Fe_3O_4-NPs in each fibers was calculated following Equation S1:

$$F_n + 0.204(1 - F_n) = R_n \quad \text{(S1)}$$

where F_n is the weight percentage of Fe_3O_4-NPs residue, the constant 0.204 is the mass fraction of none Fe_3O_4-NPs survived calculated from PDA-BF, R_n is the residual mass fraction of (PDA@Fe_3O_4-NPs)-treated fibers. The Fe_3O_4-NPs contents of F1, F2, F3, F4 and F5 are 8.0, 14.1, 19.3, 23.7 and 28.4 wt%, respectively

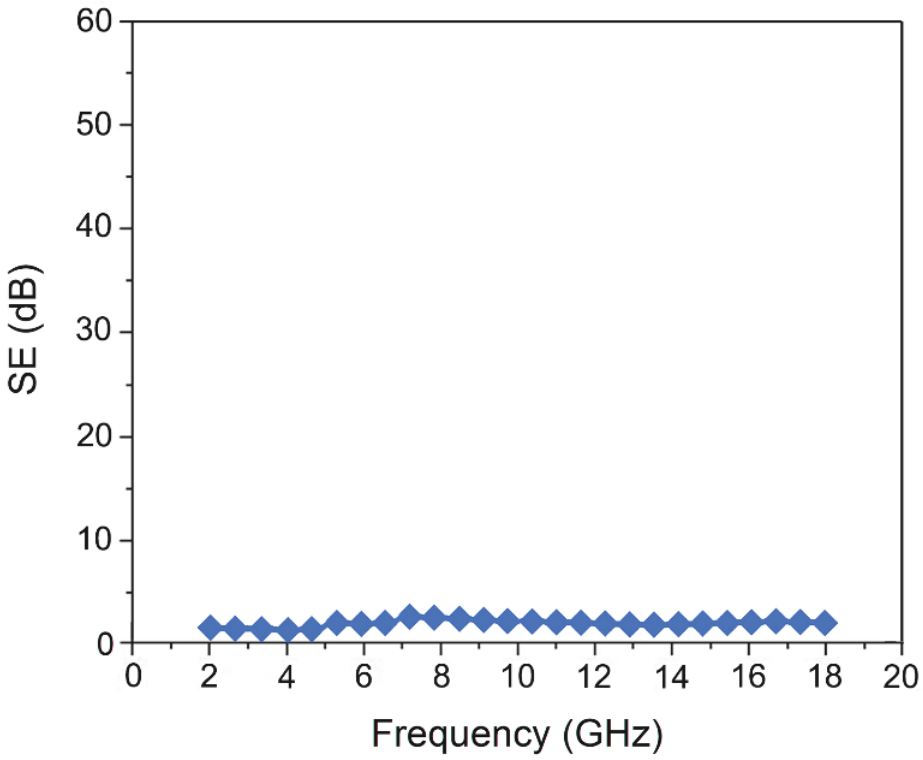

Fig. S7. SE of untreated bamboo fiber-reinforced PBS biocomposites (BF).

REFERENCES

Jiang, J., Zhu, L., Zhu, L., Zhu, B., & Xu, Y. (2011). Surface Characteristics of a Self-Polymerized Dopamine Coating Deposited on Hydrophobic Polymer Films. *Langmuir*, 27(23), 14180-14187.

Khandanlou, R., Ahmad, M. B., Shameli, K., Saki, E., & Kalantari, K. (2014). Studies on Properties of Rice Straw/Polymer Nanocomposites Based on Polycaprolactone and

Fe3O4 Nanoparticles and Evaluation of Antibacterial Activity. International Journal of Molecular Sciences, 15(10), 18466-18483.

Li, X. G., Li, A., Huang, M. R., Liao, Y., & Lu, Y. G. (2010). Efficient and Scalable Synthesis of Pure Polypyrrole Nanoparticles Applicable for Advanced Nanocomposites and Carbon Nanoparticles. *The Journal of Physical Chemistry C*, 114(45), 19244-19255.

Liu, M., Chen, C., Hu, J., Wu, X., & Wang, X. (2011). Synthesis of Magnetite/Graphene Oxide Composite and Application for Cobalt(II) Removal. *The Journal of Physical Chemistry C*, 115(51), 25234-25240.

Liu, W., Xie, T., & Qiu, R. (2016). Bamboo fibers grafted with a soybean-oil-based monomer for its unsaturated polyester composites. *Cellulose*, 23(4), 2501-2513.

Luo, J., & Gao, D. (2014). Synthesis and microwave absorption properties of PPy/Co nanocomposites. *Journal of Magnetism and Magnetic Materials*, 368, 82-86.

Wu, H., Gao, G., Zhou, X., Zhang, Y., & Guo, S. (2012). Control on the formation of Fe3O4 nanoparticles on chemically reduced graphene oxide surfaces. *CrystEngComm*, 14(2), 499-504.

Xu, G., Wang, L., Liu, J., & Wu, J. (2013). FTIR and XPS analysis of the changes in bamboo chemical structure decayed by white-rot and brown-rot fungi. *Applied Surface Science*, 280, 799-805.

Yao, L., Wang, Y., Li, Y., & Duan, J. (2017). Thermal properties and crystallization behaviors of polylactide/redwood flour or bamboo fiber composites. *Iranian Polymer Journal*, 26(2), 161-168.

Zhong, J., Gao, S., Xue, G., & Wang, B. (2015). Study on Enhancement Mechanism of Conductivity Induced by Graphene Oxide for Polypyrrole Nanocomposites. *Macromolecules*, 48(5), 1592-1597.